Cellular/Molecular

Rab11 Supports Amphetamine-Stimulated Norepinephrine Transporter Trafficking

Heinrich J. G. Matthies,[1]* Jessica L. Moore,[1]* Christine Saunders,[2] Dawn Signor Matthies,[2,8] Lynne A. Lapierre,[4,7] James R. Goldenring,[4,5,7] Randy D. Blakely,[2,3,6] and Aurelio Galli[1,6]

Departments of [1]Molecular Physiology and Biophysics, [2]Pharmacology, [3]Psychiatry, [4]Surgery, [5]Cell and Developmental Biology, [6]Center for Molecular Neuroscience, and [7]Epithelial Biology Center, Vanderbilt University School of Medicine, Nashville, Tennessee 37232, and [8]University School of Nashville, Nashville, Tennessee 37212

The norepinephrine transporter (NET) is a presynaptic plasma membrane protein that mediates reuptake of synaptically released norepinephrine. NET is also a major target for medications used for the treatment of depression, attention deficit/hyperactivity disorder, narcolepsy, and obesity. NET is regulated by numerous mechanisms, including catalytic activation and membrane trafficking. Amphetamine (AMPH), a psychostimulant and NET substrate, has also been shown to induce NET trafficking. However, neither the molecular basis nor the nature of the relevant membrane compartments of AMPH-modulated NET trafficking has been defined. Indeed, direct visualization of drug-modulated NET trafficking in neurons has yet to be demonstrated. In this study, we used a recently developed NET antibody and the presence of large presynaptic boutons in sympathetic neurons to examine basal and AMPH-modulated NET trafficking. Specifically, we establish a role for Rab11 in AMPH-induced NET trafficking. First, we found that, in cortical slices, AMPH induces a reduction in surface NET. Next, we observed AMPH-induced accumulation and colocalization of NET with Rab11a and Rab4 in presynaptic boutons of cultured neurons. Using tagged proteins, we demonstrated that NET and a truncated Rab11 effector (FIP2ΔC2) do not redistribute in synchrony, whereas NET and wild-type Rab11a do. Analysis of various Rab11a/b mutants further demonstrates that Rab11 regulates NET trafficking. Expression of the truncated Rab11a effector (FIP2ΔC2) attenuates endogenous Rab11 function and prevented AMPH-induced NET internalization as does GDP-locked Rab4 S22N. Our data demonstrate that AMPH leads to an increase of NET in endosomes of single boutons and varicosities in a Rab11-dependent manner.

Introduction

The norepinephrine transporter (NET) is a presynaptic plasma membrane protein with a critical role in the reuptake of released norepinephrine (NE) (Iversen, 1971; Pacholczyk et al., 1991; Bonisch and Bruss, 2006). The importance of NET for NE-mediated physiology and behavior is demonstrated both by the phenotypes of mice lacking NET (Bohn et al., 2000; Xu et al., 2000; Haller et al., 2002; Keller et al., 2004; Kaminski et al., 2005; Keller and Robertson, 2006) and by the consequences of polymorphisms in the human NET gene (Klimek et al., 1997; Rumantir et al., 2000; Shannon et al., 2000; Hahn and Blakely, 2002; Hahn et al., 2003, 2005, 2008; Esler et al., 2006; Kim et al., 2006; Haenisch et al., 2008). Several of these polymorphisms result in an altered level of surface NET and reduced NE transport (Hahn et al., 2003, 2005; Kim et al., 2006; Haenisch et al., 2008).

Received Sept. 15, 2009; revised March 30, 2010; accepted April 7, 2010.

This work was supported by National Institutes of Health Grants MH05892 and DA13975 (A.G.). We thank Nicole Bibus-Christianson for excellent laboratory oversight, and members of the Galli, Blakely, and Goldenring Laboratories for helpful discussions. We also acknowledge the use of the Olympus FV1000 of the Vanderbilt University Medical Center Cell Imaging Shared Resource.

*H.J.G.M. and J.L.M. contributed equally to this work.

Correspondence should be addressed to either of the following: Heinrich J. G. Matthies, Room 7141A, Medical Research Building III, Department of Molecular Physiology and Biophysics, Nashville, TN 37232-8548, E-mail: heinrich.j.matthies@vanderbilt.edu; or Aurelio Galli, Room 7124, Medical Research Building III, Center for Molecular Neuroscience, Nashville, TN 37232-8548, E-mail: aurelio.galli@vanderbilt.edu.

DOI:10.1523/JNEUROSCI.4574-09.2010

 0270-6474/10/307863-15$15.00/0

Studies over the past two decades have revealed that NET is highly regulated (Bonisch and Bruss, 2006; Mandela and Ordway, 2006). NET regulatory pathways can impact both transporter turnover rate and the level of surface NET (Apparsundaram et al., 1998a,b; Uchida et al., 1998; Bauman et al., 2000; Torres et al., 2001; Sung et al., 2003, 2005; Wersinger et al., 2006), providing mechanisms to fine-tune NE homeostasis (Bonisch and Bruss, 2006). Amphetamine (AMPH), an abused substance, also alters NE signaling, in part through actions on NET. This leads to NET-mediated NE efflux and, possibly, NET trafficking. Importantly, AMPH effects on NET may underlie vasculitis, neuropsychiatric abnormalities, and cardiomyopathy observed in abuse of the psychostimulant (Furst et al., 1990; Varner et al., 2002; Pozzi et al., 2008). Therefore, an understanding of how AMPH regulates neuronal NET including elucidation of the mechanisms and membrane compartments underlying AMPH-modulated NET trafficking may identify useful therapeutic strategies to combat the occurrence and sequelae of AMPH addiction.

A substantial portion of NET resides in intracellular vesicles of unknown nature (Leitner et al., 1999; Schroeter et al., 2000; Miner et al., 2003, 2006). Despite a previous hypothesis (Kippenberger et al., 1999; Schroeter et al., 2000; Savchenko et al., 2003), neuronal NET does not appear to sort to dense core vesicles (Leitner et al., 1999; Matthies et al., 2009) nor to several other presynaptic membrane compartments (Matthies et al., 2009). Thus, endocytic compartments are a reasonable candidate. Potential endosomal pathways include early endosomes ("rapid" rab4-positive path-

way), or recycling endosomes ("slow" rab11-positive pathway), and NET could be returned to the plasma membrane from either the "rapid" or "slow" pathway (Mellman, 1996; Robinson et al., 1996; Mukherjee et al., 1997; Novick and Zerial, 1997; Somsel Rodman and Wandinger-Ness, 2000; Zerial and McBride, 2001; Maxfield and McGraw, 2004).

Based on a preliminary observation of AMPH-induced internalization of heterologously expressed NET (Dipace et al., 2007), we hypothesized that AMPH could trigger NET internalization in neurons. In this report, we confirm this idea and demonstrate that this effect is attributable to mobilization of plasma membrane NET, in a Rab11- and Rab4-dependent manner.

Materials and Methods

Brain slice preparation and biotinylation. Brain slices were prepared from 6- to 12-week-old rats that were anesthetized with isoflurane and rapidly decapitated. After, brain removal, the brain was chilled in oxygenated ≈4°C modified artificial CSF (ACSF) (in mM: 210 sucrose, 20 NaCl, 2.5 KCl, 1 $MgCl_2$, 1.2 $NaH_2PO_4 \cdot H_2O$). The brain is then placed in a prechilled rodent brain matrix (rat; coronal slices; ASI Instruments; item RBM-4000C). Cortical slices were then collected in oxygenated ACSF (in mM: 125 NaCl, 2.5 KCl, 1.2 $NaH_2PO_4 \cdot H_2O$, 1 $MgCl_2$, 2 $CaCl_2 \cdot 2H_2O$). The slices were then transferred to a 28°C bath, allowed to equilibrate for 1 h, after which amphetamine (10 μM final) was added for 30 min. The drug reaction was terminated by removal from the bath and washing twice with oxygenated ACSF, and incubated with 4°C ACSF solution containing 1 mg/ml EZ-Link Sulfo-NHS-SS-Biotin (Pierce Chemical) for 45 min (4°C). After biotin incubation, the slices were rinsed twice quickly and for two 10 min washes in oxygenated ACSF (4°C). The reaction was quenched by washing twice for 20 min each with oxygenated ACSF containing glycine (4°C). After quenching, slices were frozen on dry ice, and the cortex was dissected and frozen at −80°C until used. Slices were lysed in 200 μl of 1% Triton buffer (25 mM HEPES, 150 mM NaCl, 2 mM sodium orthovanadate, 2 mM NaF, plus a mixture of protease inhibitors) and centrifuged at 17,000 × *g* for 30 min at 4°C. After isolation of supernatant, 400 μl of 0.1% Triton pull-down buffer (25 mM HEPES, 150 mM NaCl, 2 mM sodium orthovanadate, 2 mM NaF, plus a mixture of protease inhibitors) was added. The protein concentration was determined using a Bio-Rad protein concentration kit. Equivalent protein amounts of biotinylated proteins (supernatant) were then isolated using 50 μl of ImmunoPure immobilized streptavidin beads (Pierce) overnight at 4°C with agitation. Beads were washed three times with 0.1% Triton pull-down buffer, and biotinylated proteins were then eluted in 50 μl of 2× SDS-PAGE sample loading buffer at 95°C and then cooled to room temperature. Total slice lysates and the biotinylated (slice cell surface) fractions underwent immunodetection for NET (MAb Technologies) (Matthies et al., 2009), tyrosine hydroxylase (TH), and Na/K ATPase.

Cell culture and transfection. Mouse superior cervical ganglion neurons (SCGNs) were cultured as previously described (Savchenko et al., 2003; Matthies et al., 2009). Briefly, superior cervical ganglions were dissected from 1- to 3-d-old C57BL/6J mice and dissociated for 30 min in 3 mg/ml collagenase/0.5 mg/ml trypsin, followed by 10% FBS in DMEM. Cells were plated and incubated with 3% fetal bovine serum in UltraCulture medium containing NGF for 2 h at 37°C to allow fibroblasts to adhere. Supernatant medium (containing SCG cells) was centrifuged, resuspended in medium supplemented with FBS, and cultured on poly-D-lysine- and collagen-coated glass-bottom plates for 14 d before experiments (treating with 1 μM 5-fluoro-5-deoxyuridine after 24 h).

Cath.a-differentiated (CAD) cells are derived from transformed noradrenergic precursors that synthesize catecholamines but do not endogenously express NET (Qi et al., 1997). Human NET (hNET) was cloned into pcDNA3, stably transfected into CAD cells, and selected and maintained with 100 μg/ml G418, creating "NET cells" (Sung et al., 2003). CAD or NET cells were maintained in serum-free media to induce neuronal differentiation (Qi et al., 1997).

mCherry-Rab11-FIP2ΔC2, RFP-Rab11a, are based on previous constructs (Hales et al., 2002; Lapierre et al., 2003) but are fusion proteins of mCherry or monomeric red fluorescent protein (mRFP). mRFP and mCherry are gifts from Roger Tsien (University of California, San Diego, La Jolla, CA) mCherry-Rab11-FIP2ΔC2 and RFP-Rab11a were generated by Jennifer Schafer and Joseph Roland, respectively (Vanderbilt University, Nashville, TN). Green fluorescent protein (GFP)-NET was constructed by inserting NET into pEGFP-C2 from Clontech. Human Rab11b cDNA was isolated and cloned into mCherry vectors by standard methods. Rab11 mutants were also generated by standard methods. Transient transfections were performed using Fugene 6 reagent (Roche).

Antibodies and other reagents. Monoclonal anti-mNET (NET-05; MAb Technologies) (Matthies et al., 2009), monoclonal anti-hNET 17-1 (MAb Technologies), monoclonal anti-Na^+/K^+ ATPase α-subunit (Developmental Studies Hybridoma Bank), polyclonal tyrosine hydroxylase (Cell Signaling), polyclonal anti-Rab11a (Zymed), and polyclonal anti-Rab11a (Lapierre et al., 2001) were used at dilutions of 1:300, 1:1000, 1:100, 1:1000, 1:500, and 1:250–1:1000, respectively, for immunoblotting, with detection by enhanced chemiluminescence reaction. Monoclonal anti-mNET (NET-05; MAb Technologies) (Matthies et al., 2009), FIP1 (Hales et al., 2001), pp75/FIP5 (Hales et al., 2001), and polyclonal anti-Rab11a (as described above) were used at dilutions of 1:500, 1:110, 1:200, and 1:1000 for immunocytochemistry. Fluorescent secondary antibodies included highly cross-absorbed goat anti-mouse or anti-rabbit IgG antibodies (Invitrogen). AMPH was obtained from Sigma-Aldrich.

Cell surface protein biotinylation. Biotinylation experiments were performed on intact cells as described previously (Sung et al., 2003; Garcia et al., 2005; Dipace et al., 2007). Briefly, CAD NET cells were plated at a density of 1×10^6 per well in a six-well poly-D-lysine-coated plate. Cells were serum starved for 1 h before treatment and washed with cold PBS containing Ca^{2+}/Mg^{2+}. Then, cells were incubated with 1.0 mg/ml NHS-SS-biotin [sulfosuccinimidyl-2-(biotinamido)ethyl-1,3-dithiopropionate] (Thermo Fisher Scientific) for 30 min, washed, quenched with 100 mM glycine, and extracted in lysis buffer (PBS Ca^{2+}/Mg^{2+}, 1% Triton X-100, and 0.5 mM PMSF at 4°C). Lysates were centrifuged, total fractions were reserved, and supernatants were incubated with immobilized streptavidin beads (Thermo Fisher Scientific) for 1 h at room temperature. Beads were washed three times in lysis buffer, and bound proteins were eluted with 2× sample buffer containing 2-mercaptoethanol. Proteins were separated by SDS-PAGE and immunoblotted. For estimation of relative amounts of proteins, the exposed films of the immunoblots were scanned, and band intensities were measured with Scion Image (Scion Corporation).

Immunostaining. SCG neurons were serum starved for 1 h in DMEM: F12 and treated with vehicle or AMPH for 10 or 30 min. Neurons were subsequently fixed with PBS Ca^{2+}/Mg^{2+}/4% paraformaldehyde, washed three times with PBS Ca^{2+}/Mg^{2+}, permeabilized, and blocked with PBS/4% bovine serum albumin (BSA)/0.15% Tween 20, and immunostained with the appropriate antibody dissolved in PBS plus 4% BSA and 0.05% Tween 20. Primary antibodies were visualized with the appropriate covalently Alexa-labeled secondary antibody from Invitrogen. Immunofluorescence was imaged by capturing *Z*-series using a PerkinElmer UltraView confocal with a Nikon Eclipse 2000-U microscope equipped with a 60× lens with numerical aperture (NA) of 1.49, or an Olympus FV 1000 using a 60× lens with NA of 1.45 (Vanderbilt University Medical Center Cell Imaging Shared Resource). All images shown are always from single confocal sections, and image processing was performed using ImageJ and Adobe Photoshop.

Analysis of NET internalization. The quantitation of NET intracellular accumulation was achieved using pixel intensity plots of a single confocal section along a line through the center of each bouton using ImageJ. The line intersects the brightest spot on one side of the widest portion of the bouton perimeter. The line was extended beyond the limits of the bouton to generate a background value, and then divided into 20 bins (bin 10 is approximately at the center of the bouton) for the pixels spanning the bouton. NET fluorescence intensity of each bin was normalized to the fluorescence intensity of the brightest spot on the bouton perimeter (100%), and the mean ± SEM pixel intensity of each bin was plotted.

Colocalization analysis. Colocalization analysis was performed as previously described (Matthies et al., 2009) following protocols established by Stanley and coworkers (Li et al., 2004). Only images in which there was

no pixel saturation were analyzed. Background fluorescence was first subtracted in ImageJ by selecting an unstained area of each image and running the background subtraction plug-in available at http://www.uhnresearch.ca/facilities/wcif/fdownload.html. The intensity correlation quotient (ICQ) was then determined by running the intensity correlation analysis (ICA) plug-in for ImageJ developed by Tony Collins and Elise Stanley (Toronto Western Research Institute, Toronto, ON, Canada), also available at the above link. The ICQ indicates whether the intensity of staining for two proteins varies in synchrony over space. An ICQ value of +0.5 means that, in any pixel with a certain intensity of staining for one protein, the intensity of staining for the other protein studied will be exactly the same, whereas an ICQ value of 0 signifies no relationship between the two staining patterns. An ICQ value of −0.5 indicates an inverse relationship for colocalization.

To determine and visualize sites of colocalization, software at the above link was used to generate images with psudocolored pixels and points where values for both antigens have pixel values above the mean (Li et al., 2004). In the software, these images are called +ves and are images of pixels that have positive PDM (product of the differences from the mean) values resulting from both pixels above the mean (i.e., red intensity minus mean red intensity and green intensity minus mean green intensity are both positive) (http://www.uhnresearch.ca/facilities/wcif/fdownload.html).

Density gradient centrifugation. NET cells were homogenized in PBS (cleared of intact cells and nuclei by centrifugation at 1000 × *g* for 10 min) and then mixed with OptiPrep (iodixanol) (Ford et al., 1994; Graham et al., 1994; Billington et al., 1998) to a final concentration of 13% and loaded into Sorvall Ultracrimp tubes. Centrifuging at 60,000 rpm in a vertical 70V6 rotor in a Sorvall Ultra 80 produced a density gradient. The 400 μl fractions were collected by displacement, and their density was calculated from manually measured refractive indices (Ford et al., 1994; Graham et al., 1994; Billington et al., 1998). Proteins in all fractions were separated by SDS-PAGE and immunoblotted for NET, Rab11a, Rab4, Rab5, and/or Na/K ATPase, and an estimation of the relative intensity of the relevant protein per fraction were determined as described for biotinylation experiments. Relative amounts of a protein in each fraction were plotted as fractions relative to the total (sum of all fractions).

Results

In rat cortical slices, AMPH decreases surface NET

In initial studies using a heterologous expression system, we observed that AMPH caused trafficking of NET away from the plasma membrane (Dipace et al., 2007). Here, we used a brain slice preparation that contains noradrenergic terminals to test the hypothesis that AMPH reduces surface NET. Rat cortical brain slices were incubated either with vehicle or 10 μM AMPH for 30 min (Fig. 1*A*). We found that AMPH decreased the surface expression of NET. Shown are representative immunoblots of biotinylated and total fractions treated with either vehicle (CTR) or 10 μM AMPH (AMPH) (Fig. 1*A*). Quantitation of AMPH-induced NET surface expression demonstrates a significant decrease compared with control (72.6 ± 14.8%). The biotinylated band intensities are normalized to total NET and expressed as percentage of control conditions (Student's *t* test, $p \leq 0.05$; $n = 13$). TH, a cytosolic protein, is detected primarily in the total fraction and comprises <1% of the surface fraction. In addition, representative Western blots of surface and total Na^+/K^+ ATPase levels are shown to serve as a loading control. Therefore, these data demonstrate that the biotinylated fraction represents cell surface proteins and speak to the health of noradrenergic TH-positive neurons in the assay. These studies suggest that AMPH treatment leads to a reduction of surface NET in noradrenergic projections in the context of a native environment.

In boutons of SCGNs, AMPH increases cytoplasmic NET as well as NET and Rab11a colocalization

Since NE is predominantly released at presynaptic sites, we asked whether AMPH application modifies NET surface expression within single boutons (a presynaptic site) of differentiated SCG neurons. We recently developed a new rodent-specific NET antibody allowing us to adopt mouse SCGNs as a model system to study NET distribution in boutons (Matthies et al., 2009). Some of the boutons of SCGNs are ideal for optical studies because of their large diameter (Matthies et al., 2009). These boutons (2–4 μm diameter) are active sites of membrane recycling likely including NE release, since high K^+-induced depolarization leads to FM1-43 labeling (data not shown). Under basal conditions, NET is enriched at the perimeter of SCGN boutons (Fig. 1*B*, top two images). Application of AMPH (10 μM; 30 min) leads to increased NET immunoreactivity in the interior of the boutons (Fig. 1*B*, bottom two images). These results indicate that AMPH causes internalization of NET in neurons.

We quantified these observations using pixel intensity plots of a single confocal section. For the image analysis, a straight line was drawn across the widest portion of each approximately spherical bouton, intersecting the brightest spot of fluorescence on one side of the bouton, and the fluorescence on the opposite side. The resulting line spanned the full diameter of the bouton and was extended beyond the limits of the bouton to generate a background value (see Materials and Methods). The line spanning the bouton was then divided into 20 bins (with bin 10 at approximately the center of the bouton), thereby binning the pixels spanning the bouton. The NET fluorescence intensity of each bin was normalized to the fluorescence intensity of the brightest spot (100%), and the mean ± SEM pixel intensity of each bin was plotted. Figure 1*C* shows that, in AMPH-treated neurons, intrabouton fluorescence signal was significantly elevated over that found in untreated boutons, validating intracellular accumulation of NET with AMPH treatment (two-way ANOVA, followed by Bonferroni's post tests, $^*p < 0.05$, $^{**}p < 0.01$, $^{***}p < 0.001$).

Our hypothesis is that AMPH leads to a reduction in NET plasma membrane expression via enhanced NET trafficking through endosomes. Our previous results (Dipace et al., 2007) suggested that the kinetics of NET internalization might be slow, implying the role of the slow recycling Rab11-positive pathway. Therefore, we analyzed NET colocalization with Rab11 as well as with Rab4, which is a marker for the sorting endosome, after 30 min of AMPH exposure. One accepted function for both of these Rab proteins is their role for the recycling back to the plasma membrane. Here, we determined in SCGN boutons whether Rab4 and Rab11 colocalization with NET is altered by AMPH exposure (Fig. 1*D–F*). NET and Rab4 do not colocalize under basal (CTR) conditions (Fig. 1*D*, CTR, top row). However, AMPH increased colocalization between a subset of Rab4 organelles and NET (Fig. 1*D*, AMPH, bottom row). Next, we compared the distribution of NET and Rab11a in control and AMPH-treated SCGN boutons (Fig. 1*E*). Although there is uncertainty as to whether Rab11a is present in presynaptic terminals (Sheehan et al., 1996), we detected the protein in SCGN boutons. Moreover, under control conditions, we observed colocalization between Rab11a and NET at the juxtamembrane region. Generally, Rab11a was found just cytoplasmic to the most abundant NET staining at the plasma membrane (Fig. 1*E*, top row, arrows). The intensity of NET in the juxtamembrane region was much lower than on the perimeter of the bouton. In contrast, in AMPH-treated neurons, we detected a significant increase in colocalization between NET and Rab11a in

regions both in the center, just below, and on the perimeter of the bouton (Fig. 1*E*, bottom row, arrows). These apparent AMPH-induced increases in colocalization between NET, Rab4, and Rab11a were quantitated using the ICA/ICQ method (Li et al., 2004) as described in Materials and Methods (Fig. 1*F*). In the basal state, we determined that the ICQ value for NET and Rab4 is close to zero (-0.013 ± 0.03) indicating a random distribution. On AMPH treatment, the ICQ value is significantly increased (0.103 ± 0.02; $^{**}p \leq 0.001$, Student's *t* test; $n = 12$), indicating dependent staining of Rab4 and NET (Fig. 1*F*). Rab11a and NET displayed some colocalization under the basal state, which was significantly enhanced (from 0.104 ± 0.02 to 0.205 ± 0.02) on AMPH exposure ($^{*}p \leq 05$, Student's *t* test; $n = 13$) (Fig. 1*F*). To further support the presence of Rab11a at presynaptic terminals, we determined whether identified Rab11a effectors and binding proteins Rab11-FIP1, Rab-FIP2, and Rab11-FIP5 (Prekeris et al., 2000; Hales et al., 2001) are expressed at SCGN boutons. Rabs are GTPases that lead to specificity of membrane trafficking via the nature of the bound guanosine nucleotide. Rabs bind to effectors depending on the hydrolysis state of the bound nucleotide, and the Rab/effector interaction leads to docking/tethering at fusion sites or vectorial transport using various cytoskeletal elements (Mellman, 1996; Robinson et al., 1996; Zerial and McBride, 2001; Maxfield and McGraw, 2004; Jordens et al., 2005; Grosshans et al., 2006). Here, we show (Fig. 1*G*,*H*) that several Rab11 effectors including Rab-FIP1, Rab11-FIP2 (data not shown), and Rab11-FIP5 are found in SCGN boutons, further supporting the functional presence of Rab11a and its signaling partners in presynaptic neuronal compartments. Rab11-FIP1, Rab11-FIP2 (data not shown), and Rab11-FIP5 were also detected just below the NET demarcated perimeter and in the interior of the bouton (Fig. 1*G*,*H*). Our results demonstrate that Rab11a and its effectors are present in these synaptic terminals, consistent with previous work that identified Rab11-FIP2 and Rab11-FIP5 as phosphoproteins in synaptosomes (Collins et al., 2005, 2008). In addition, these data provide support to our hypothesis that Rab11a coordinates AMPH-induced NET trafficking.

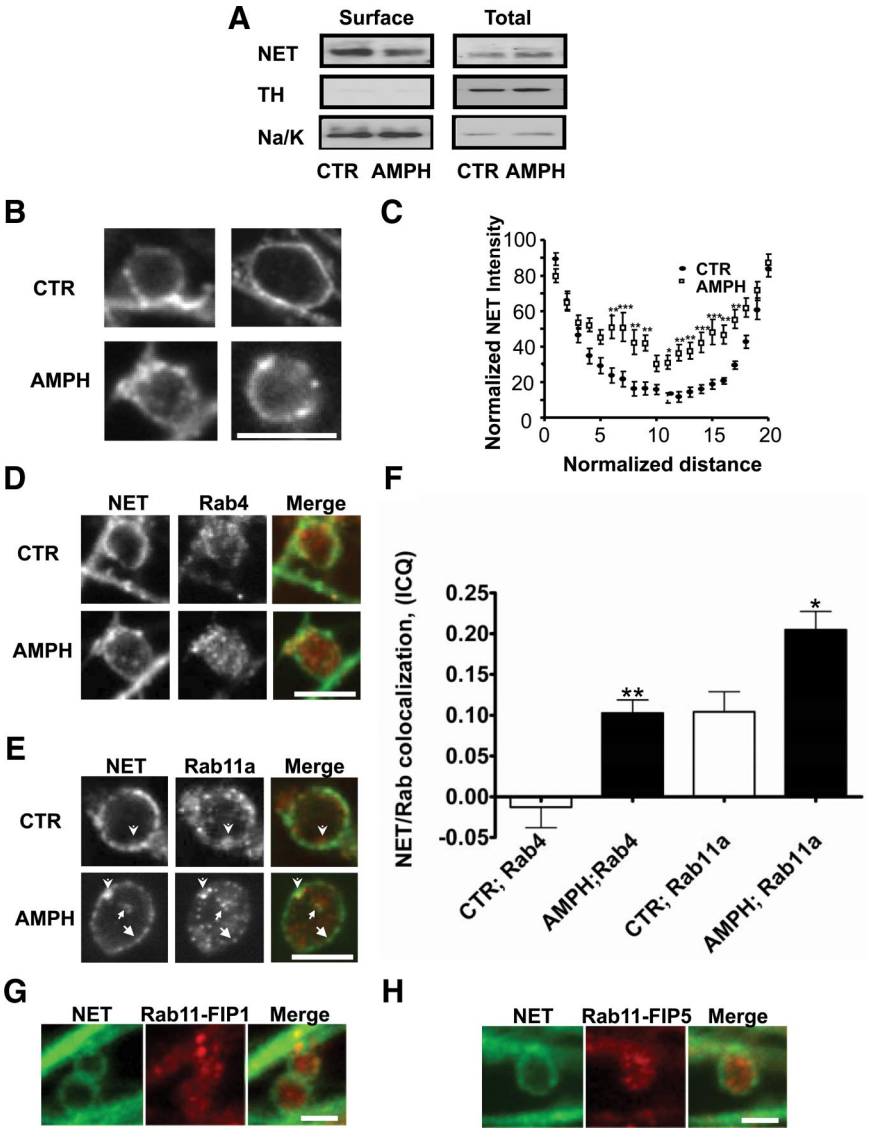

Figure 1. Amphetamine leads to a decrease in surface NET expression in rat cortical slices and NET in boutons and colocalization of NET with Rab11a and Rab4. ***A***, Representative immunoblots of surface and total NET from biotinylated rat cortical slices. 300 μm rat cortical slices [paired right vs left hemispheres for vehicle (CTR) vs AMPH] were incubated for 30 min with 10 μM AMPH and then biotinylated (see Materials and Methods). A volume of 25 μl of total slice lysate was loaded per sample (lane). A volume of 45 μl of eluted (biotinylated proteins) was loaded per sample (lane). Tyrosine hydroxylase and Na/K ATPase immunoreactivity was also probed. A total of 13 cortical slices from three rats were analyzed. $^{*}p < 0.05$ by Student's *t* test. Mouse SCGNs were cultured and processed for immunocytochemistry as described in Materials and Methods. ***B***, SCGNs treated with 10 μM AMPH for 30 min leads to an accumulation of intracellular NET in SCGN boutons. Images are taken from single confocal and depict single boutons with associated axons (linear structures). The perimeter of the boutons is marked by intense NET immunoreactivity, as well as intrabouton immunoreactivity, which is increased by AMPH. ***C***, Analysis of intensity plots spanning SCGN boutons demonstrates that AMPH treatment induces NET accumulation in the interior of these boutons. The normalized NET intensity is plotted against the normalized distance as described in Materials and Methods. ***D***, AMPH treatment of SCGNs enhances NET and Rab4 colocalization in boutons. Shown in the top row are boutons from cultures treated with vehicle (basal state). Shown in the bottom row are AMPH-stimulated cells showing colocalization between NET and Rab4. ***E***, AMPH treatment of SCGNs enhances NET and Rab11a colocalization in boutons. Shown in the top row are boutons from cultures treated with vehicle (basal state), and arrowheads indicate colocalization of NET and Rab11a at a juxtaplasma membrane location. The intensity of the juxtaplasma membrane NET is lower than on the perimeter. Shown in the bottom row are AMPH-stimulated cells with arrows pointing to surface (arrows), juxtaplasma membrane (arrowhead), and internal (small arrow) regions showing colocalization between NET and Rab11a. ***F***, Quantitation of NET and Rab11a, Rab4 colocalization using the ICQ as outlined in Materials and Methods (Li et al., 2004) demonstrates that AMPH enhances the colocalization of NET and Rab11a as well as Rab4. ***G***, ***H***, Rab11a effectors are present in the presynaptic compartments of SCGN. Scale bar, 5 μm. Error bars indicate SEM.

AMPH-induced NET redistribution assessed by subcellular fractionation

We next sought biochemical confirmation of AMPH-induced NET trafficking through Rab11a positive compartments and returned to the NET-transfected CAD model (NET cells) to explore the distribution and density of NET membranes in the presence and absence of AMPH. AMPH-induced changes in NET cell surface expression were evaluated by biotinylation assays, and density gradient fractionation was used to ascertain both NET

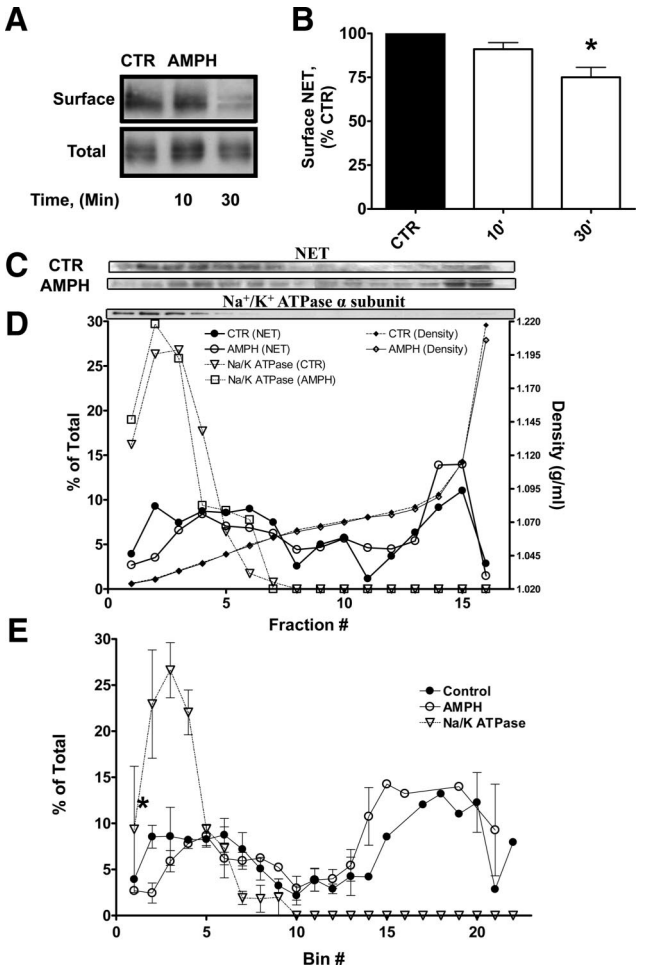

Figure 2. AMPH-induced loss of NET from the cell surface and redistribution to intracellular organelles characterized by cell fractionation. ***A***, AMPH treatment (10 μM) of NET cells leads to a reduction of the intensity of NET in the biotinylated fraction. Shown is a representative Western blot. ***B***, Quantitation of an AMPH-induced decrease of NET in the biotinylated fraction. Biotinylated band intensities are normalized to total NET and expressed as percentage of control (Student's *t* test, $*p \leq 0.05$; $n = 7$). ***C***, AMPH treatment of NET cells for 30 min leads to a redistribution of NET away from a light plasma membrane fraction. Top, Shown are immunoblots of NET from either vehicle- or AMPH (10 μM)-treated NET cells from various fractions of an OptiPrep gradient (low-density fractions on the left; denser fractions on right). Below is an immunoblot of Na/K ATPase, a plasma membrane protein, which we used to identify plasma membrane fractions. ***D***, A plot of the percentage in each fraction of total NET intensity obtained from NET cells treated with AMPH (open circles) or vehicle (filled circles). The percentage of the total intensity of the Na/K ATPase (open triangles) in various fractions is also shown. The right *y*-axis indicates the density of the fractions of the OptiPrep gradient from lysates treated with AMPH (open diamonds) or vehicle (filled diamonds). ***E***, Graph averaging the results of NET immunoblots obtained as in ***D*** from three independent OptiPrep gradients. Error bars indicate SEM.

redistribution and colocalization with Rab11a. In NET cells, 10 μM AMPH induces a significant reduction in surface NET in 60 min (Dipace et al., 2007), and we confirmed this result at 30 min. Figure 2*A* shows representative immunoblots of biotinylated and total fractions from NET cells treated with either vehicle (CTR) or 10 μM AMPH (AMPH) for 10 and 30 min at 37°C. At 30 min, AMPH decreases plasma membrane expression of NET without changes in total NET. Figure 2*B* displays the quantitation of AMPH-induced decrease in NET surface expression. The biotinylated band intensities are normalized to total NET and expressed as percentage of control conditions (Student's *t* test, $*p \leq 0.05$; $n = 7$).

Next, we assessed the density of NET-containing organelles in relation to proteins for various subcellular organelles using density gradient centrifugation (OptiPrep medium). Figure 2*C*, top, shows representative immunoblots displaying the distribution of NET across the OptiPrep gradient from NET cells treated either vehicle (CTR) or with 10 μM AMPH for 30 min (AMPH). In addition, an immunoblot of the plasma membrane marker Na^+/K^+ ATPase α-subunit (Na^+/K^+ ATPase α-subunit) is displayed. Figure 2*D* displays the quantitation of the intensity of NET immunoreactivity in each fraction. The density of the fractions is identified by diamond symbols and corresponds to the values on the right *y*-axis. Fractions at lighter densities (1.02–1.06 g/ml) contained a substantial proportion of NET under control conditions (solid circles). Based on previous work, some of these lighter fractions likely contain plasma membranes (Graham, 2001). This was confirmed by the presence in these fractions of the Na^+/K^+ ATPase α-subunit (open triangles). On treatment with AMPH, the distribution of NET displayed a shift to higher density fractions (1.07–1.13 g/ml) lacking the Na^+/K^+ ATPase α-subunit and substantially decreased in a light plasma membrane fraction (open circles). We divided the gradient into 22 bins based on fraction density, allowing for the averaging of fractions from multiple experiments. Figure 2*E* represents the average of three experiments. Consistent with Figure 2*D*, AMPH (open circles) decreased NET intensity in the light plasma membrane fractions with respect to vehicle-treated control (solid circles). Thus, NET in a light plasma membrane fraction (fraction 3) was decreased by ~60%, based on peak height (Student's *t* test, $p \leq 0.01$), from 7.6 ± 0.9101% in control conditions to 2.3 ± 0.6450% on AMPH treatment.

AMPH increases colocalization of NET with Rab11a and Rab4

Figures 1 and 2 show that AMPH causes cell surface redistribution of NET and increased colocalization of NET with Rab11a and Rab4. We have also demonstrated that, under basal conditions, NET resides in Rab11a-positive compartments (Fig. 1) and that AMPH induces increased colocalization with both Rab4- and 11a-positive structures (Fig. 1). We next sought to determine whether Rab11a is in the same density fractions as NET in vehicle- or AMPH-treated NET cells (Fig. 3). Therefore, immunoblots from density gradients from either vehicle- or AMPH-treated NET cells were probed for Rab11a.

Figure 3*A* shows immunoblots of Rab11a (top) for vehicle- and AMPH-treated cells, and quantitation of the intensity of the immunoreactivity of the different density fractions (bottom). Figure 3*B* represents an average distribution of Rab11a from three independent experiments. Rab11a exists in both low-density and high-density fractions (Fig. 3*A*). On AMPH treatment, Rab11a levels tend to increase in low-density fractions (Fig. 3*A*,*B*), which have been shown by others to correspond to the densities of both early and recycling endosomes in OptiPrep gradients (Herman et al., 1994; Sheff et al., 1999; Hashiramoto and James, 2000; Proikas-Cezanne et al., 2006). These data suggest that, in addition to promoting colocalization of Rab11a and NET, AMPH also leads to the redistribution of both NET and Rab11a to fractions with similar density.

AMPH treatment also led to increased colocalization of NET with Rab4. Therefore, we probed gradient fractions for Rab4. Under control or basal conditions, a substantial portion of Rab4 was observed in high-density fractions (Fig. 3*C*). Figure 3*C* shows a representative immunoblot of Rab4 from vehicle-treated cells and quantitation of the intensity of the immunoreactivity of the different density fractions (bottom). Approximately 60% of Rab4

is in fractions with high densities. In other cell types, the level of Rab4 at these high densities is below the threshold of detection (Proikas-Cezanne et al., 2006), whereas in cells expressing regulated secretory vesicles, such as Glut4 storage granules and NET cells as shown here, two peaks of Rab4 are detected with a substantial peak at high densities (Herman et al., 1994; Hashiramoto and James, 2000; Lim et al., 2001).

AMPH treatment caused some redistribution of Rab11a (Fig. 3*A*,*B*) in density gradients, but major effects on the distribution of Rab4 were not noted (data not shown). Rab4 is enriched in three peaks and NET is found in these fractions, particularly in the densest peak. On AMPH exposure, more NET tends to be in these dense fractions (Figs. 2*D*,*E*, 3*C*).

To better characterize the distribution of NET relative to markers of other well characterized trafficking compartments, we probed immunoblots of OptiPrep gradients with antibodies against early endosome markers (Rab5) and late endosomes/lysosomes (LAMP1). The majority of Rab5 was present in possibly three peaks, one at a light density and two overlapping peaks at high density. The lighter peak does not coincide with a fraction with major changes in NET levels on AMPH treatment. Indeed, AMPH-induced increases in NET are found in denser fractions with high levels of Rab5. In contrast, LAMP1 immunoreactivity was found in many fractions. However, the fractions in which AMPH leads to enhanced levels of NET do not coincide with a LAMP1 peak fraction.

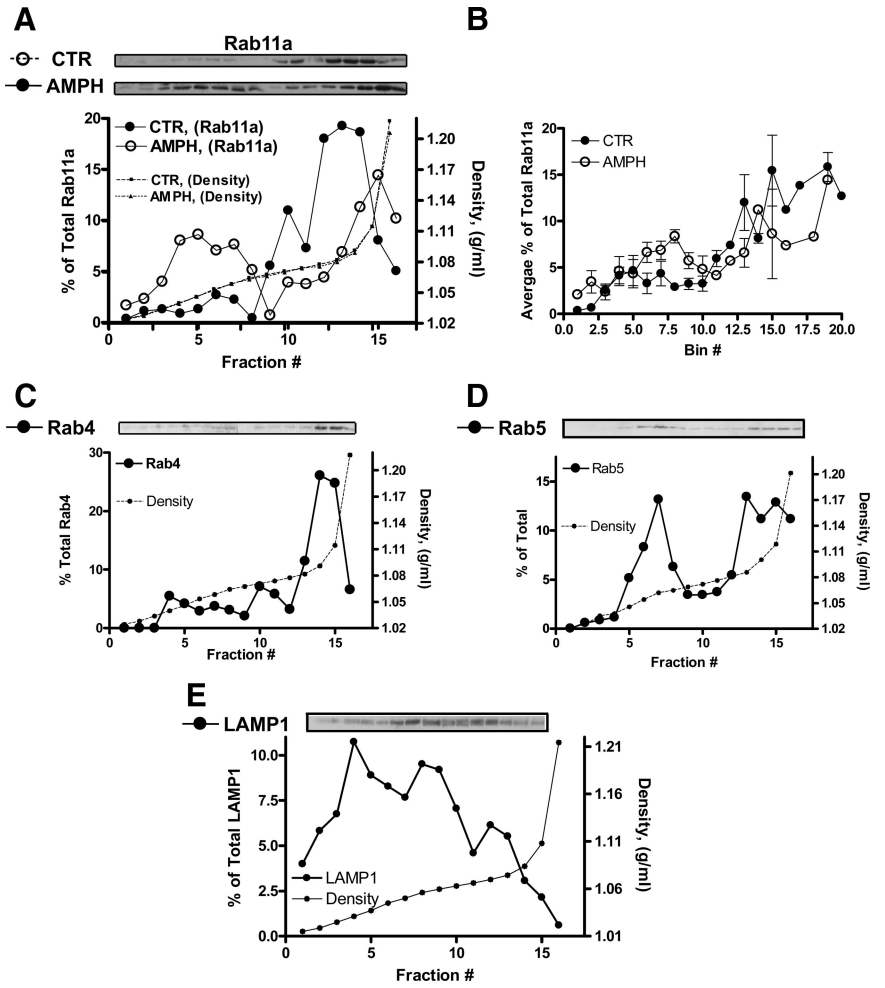

Figure 3. Rab11a-containing fractions have similar densities to NET-containing fractions in both control and AMPH-treated cells. ***A***, Top, Displayed are immunoblots of fractions from OptiPrep gradients used to fractionate extracts from control vehicle-treated (CTR) or AMPH-treated NET cells. Less dense fractions are on the left, whereas denser fractions are on the right side of the immunoblot. Bottom, Quantitation of the immunoblots. Plotted is the percentage of the total Rab11a loaded into the gradient versus the fraction number. AMPH leads to accumulation of Rab11a in lighter fractions. ***B***, Shown is a plot representing the quantitation of three independent experiments. In this plot, the percentage of the total Rab11a loaded into the gradient is on the *y*-axis, and the *x*-axis represents bins generated based on the density of each fraction (see Materials and Methods). ***C–E***, Marker for early (Rab4, Rab5) and late (LAMP1) endosomal fractions are shown. Error bars indicate SEM.

At early time points of AMPH treatment of SCGNs, NET is found adjacent to sites where clathrin and Rab11a colocalize

We have previously noted that concentrated NET puncta are preferentially found in sites with intense syntaxin 1 immunoreactivity, and in domains marked by cholera toxin, which are most likely lipid rafts (Matthies et al., 2009). Interestingly, syntaxin 1 is also known to be partially found in lipid rafts (Chamberlain et al., 2001; Lang et al., 2001). Because syntaxin 1 is a protein with a major role in exocytosis, these data suggest that a fraction of NET is in exocytotic domains that are likely lipid rafts. We also note that, occasionally, Rab11a- and Rab11-binding proteins are observed just below surface NET puncta at boutons (Fig. 1). Rab11a, which we observe adjacent to NET puncta (Fig. 1), has been suggested to play a role in exocytosis at the stage of vesicle tethering (Zhang et al., 2004; Jafar-Nejad et al., 2005; Langevin et al., 2005; Lim et al., 2005; Savina et al., 2005; Wu et al., 2005; Oztan et al., 2007). In addition to a possible function in exocytosis, Rab11a could also function in endocytosis. Importantly, distinct endocytic sites not overlapping with exocytotic domains have been described in presynaptic areas (Roos and Kelly, 1999). Therefore, we compared the distribution of NET with a marker of endocytic sites (clathrin) and with Rab11a in SCGN boutons (Fig. 4).

We exposed SCGNs cultures to 10 μM AMPH for 10 min to observe NET early trafficking events, thereby allowing us to determine the distribution of "exocytotic and endocytic sites" in the same bouton. Figure 4*A* shows triple-stained confocal sections for NET, clathrin, Rab11a, and triple merged, spanning an entire one-half of several boutons starting from the center (left) and scanning to the bottom (right). These images demonstrate that AMPH-treated boutons show both NET puncta at the plasma membrane (Fig. 4*A*, top row) and clathrin clustering. This is suggestive of clathrin assembly at presynaptic sites (Fig. 4*A*, second row). To determine whether plasma membrane NET resides in the clathrin endocytic domains, we merged NET and clathrin images in Figure 4*B*, top row. We found low but significant colocalization of NET and clathrin ($^*p \leq 0.05$; $n = 17$) and clathrin tended to surround surface NET puncta. These sites of colocalization between NET and clathrin were visualized computationally as outlined in Materials and Methods by displaying an image in which pixels for both antigens have pixel values above the

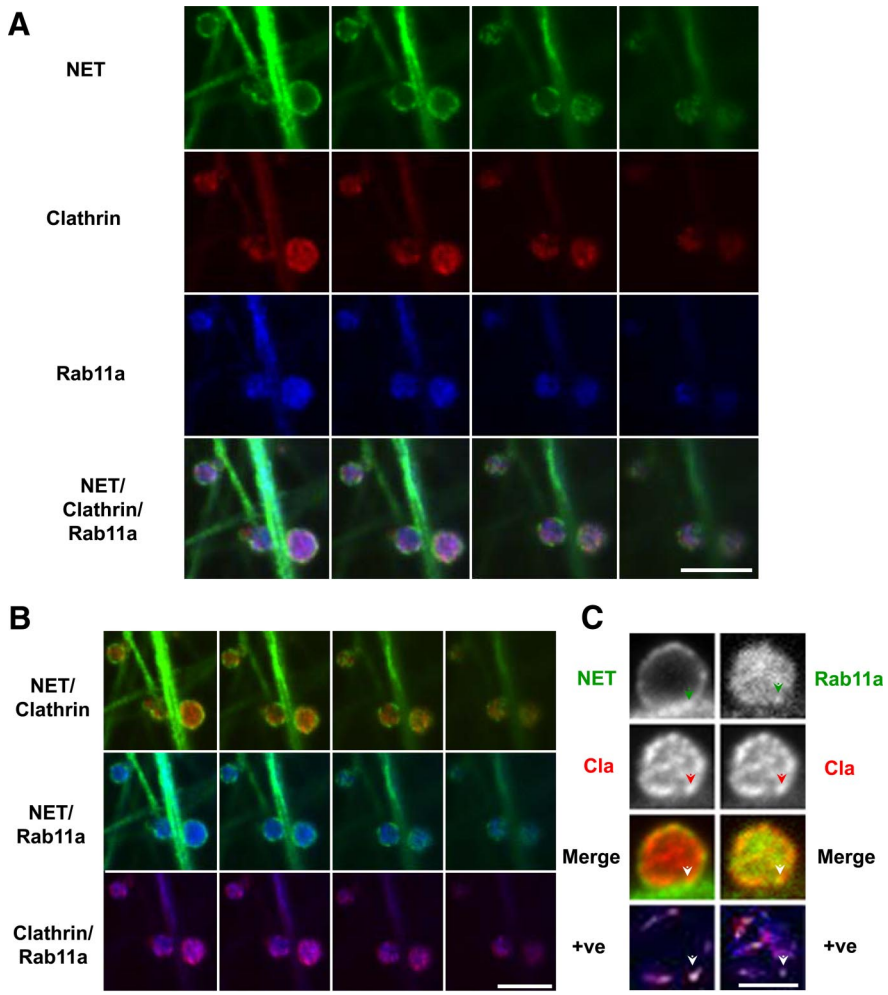

Figure 4. At early time points of AMPH treatment of SCGNs, Rab11a colocalizes with clathrin at juxtaplasma membrane and internal sites. Mouse SCGNs were cultured, treated with vehicle or AMPH (10 μM) for 10 min, and processed for immunocytochemistry as described in Materials and Methods. All images are taken from single confocal sections. Cultures were treated with vehicle or AMPH (10 μM) for 10 min. At this time point, low levels of NET are internalized (Fig. 2). ***A***, In this panel, single confocal sections spanning the boutons from the center to the bottom are displayed. They are tripled labeled for NET, clathrin, and Rab11a. The merge of the triple-labeled sections is shown in the fourth row. Scale bar, 2.5 μm. ***B***, Displayed are the double-merge images of the same sections as in ***A***. Some colocalization of clathrin with NET is detected at the edges of NET puncta (top row), and low levels of NET and Rab11a can be seen at the perimeter (middle row). Finally, clathrin and Rab11a are highly colocalized both at the surface and in the interior (bottom row). Scale bar, 2.5 μm. ***C***, In this panel, single confocal sections at the center to the bottom are displayed. This section was tripled labeled for NET (NET), clathrin (Cla), and Rab11a (Rab11a). For the sake of comparison, the double-merged image was generated by pseudocoloring both NET and Rab11a red, whereas clathrin was green. In the bottom row are images that display pseudocolored pixels from the images of boutons in which the pixel values for the two relevant antigens are both above the mean. An arrowhead indicate a site in which both NET/clathrin colocalize and Rab11a/clathrin colocalize based on analyzing the two images in the bottom panel (see Materials and Methods). Scale bar, 2.5 μm.

mean (Fig. 4*C*, bottom row, left column; +ve). Most intense sites of colocalization approach white, whereas sites with low values are black. Colocalization at one site is marked by an arrowhead in the NET, clathrin merge, and +ve images, respectively.

In Figure 1, we show that 30 min of AMPH increased colocalization between Rab11a and NET and that this increase occurs in part at the plasma membrane in juxtamembrane regions. To determine whether this colocalization occurs at the early time points of AMPH-induced NET trafficking, we merged NET and Rab11a images after 10 min of AMPH exposure. Figure 4*B*, second row, shows modest colocalization between these two proteins at the membrane, in contrast to what we observed after 30 min of AMPH. The question remained whether clathrin and Rab11a colocalized in endocytic compartments. Figure 4*B*, bottom row, shows high colocalization between clathrin and Rab11a. Furthermore, we detected overlap of Rab11a and clathrin on internal sites, which may suggest clathrin assembly on endosomes (van Dam and Stoorvogel, 2002; van Dam et al., 2002; Pagano et al., 2004). All sites of colocalization of Rab11a and clathrin were further visualized by displaying an image with pseudocolored pixels at points where values for both antigens (Rab11a and clathrin) have pixel values above the mean (Li et al., 2004) (Fig. 4*C*, bottom row of right column; +ve) as above for NET and clathrin. Most intense sites of colocalization approach white, whereas sites with low values are black. Colocalization at one site is marked by an arrowhead in the Rab11a, clathrin merge, and +ve images, respectively. In addition, there was also diffuse Rab11a staining that did not overlap with clathrin (Fig. 4*B*, note blue in bottom row). At this early time point, intrabouton NET immunoreactivity appeared in a diffuse pattern consistent with endocytic vesicles, which typically have diameters in the 40–70 nm range. We determined overlap in these two images in the bottom row of Figure 4*C* as outlined in Materials and Methods (data not shown), indicating some sites exist where both NET/clathrin or Rab11a/clathrin colocalization overlap (Fig. 4*C*, arrowhead indicates a site). These sites are where NET colocalizes with Rab11a and appear to be endocytic sites as indicated by the presence of clathrin.

A fraction of NET and Rab11a sort to the same organelles

To test the hypothesis that Rab11a is required for the delivery of NET to the recycling endosome, we overexpressed a Rab11a fusion protein to perform live-cell imaging. It has been shown that the overexpression of Rab11a can lead to the coaccumulation of Rab11a and some endocytic cargo in recycling endosomes, which are typically found in a perinuclear position (Ullrich et al., 1996; Ren et al., 1998). Therefore, if NET traffics via the recycling endosome, overexpression of Rab11a in CAD cells should lead not only to the colocalization of NET and Rab11a, but also their synchronous movement in living cells. We expressed GFP-NET together with RFP-Rab11a (see Materials and Methods) and found that the overexpression of Rab11a leads to GFP-NET and RFP-Rab11a accumulation in a perinuclear position (Fig. 5*A*, top row, arrows). Importantly, in axonal swellings, both GFP-NET and RFP-Rab11a were observed in organelles with similar morphologies (Fig. 5*A*, bottom row, arrows). In addition, we noticed diffuse NET and Rab11a both in the cell bodies and at axonal swellings (Fig. 5*A*,*B*). In time series, it was evident that doubly labeled organelles move in synchrony,

establishing that both NET and Rab11a can be sorted to the same organelle in living cells (Fig. 5*B*, arrows).

Previous studies have shown that Rab11a is required at multiple levels during the trafficking of cargo, including the delivery of endocytic cargo to recycling endosomes, and from the recycling endosome to the plasma membrane (Ullrich et al., 1996; Ren et al., 1998; Wang et al., 2000; Hales et al., 2002; Schonteich et al., 2008). This was demonstrated mainly by disrupting Rab11a function (Ullrich et al., 1996; Ren et al., 1998; Wang et al., 2000; Hales et al., 2002; Schwenk et al., 2007; Welsh et al., 2007; Schonteich et al., 2008; Eggers et al., 2009). To discriminate between the different roles of Rab11a in the trafficking of NET, we used a truncated version of the Rab11 effector protein Rab11-FIP2 lacking the C2 domain (FIP2ΔC2) (Hales et al., 2002). The C2 domain of FIP2 may have lipid binding activity (Lindsay and McCaffrey, 2004). Expression of FIP2ΔC2 severely disrupts Rab 11 distribution and plasma membrane recycling (Hales et al., 2002; Lindsay and McCaffrey, 2002, 2004; Fan et al., 2004). It was previously shown that FIP2ΔC2 accumulates in the recycling endosome (Hales et al., 2002). Therefore, the prediction is that, if the earliest disrupted step requiring Rab11 is the delivery of NET to the plasma membrane, then NET and FIP2ΔC2 will colocalize in the recycling endosome. Importantly, if the earliest Rab11 requirement is delivery of NET to the recycling endosome, then NET and FIP2ΔC2 should not colocalize. Therefore, we examined live CAD cells expressing GFP-NET and either mCherry-FIP2ΔC2 or mCherry alone. In control cells, GFP-NET was found in the cell body (Figs. 5, 6), axonal swellings (Fig. 6), and neurites (Fig. 4). In axonal swellings, we detected NET on the surface and in the interior (Fig. 6*A*). A fraction of NET had a diffuse appearance (Fig. 6*A*). We also saw regions of concentrated NET-bearing organelles that moved in partial synchrony over time, particularly in the center of axonal swellings (Fig. 6*A*, $t = 0$ to $t = 3$). In these highly concentrated regions of GFP-NET, we noted lower densities of mCherry, strongly suggesting that mCherry does not randomly colocalize with GFP-NET.

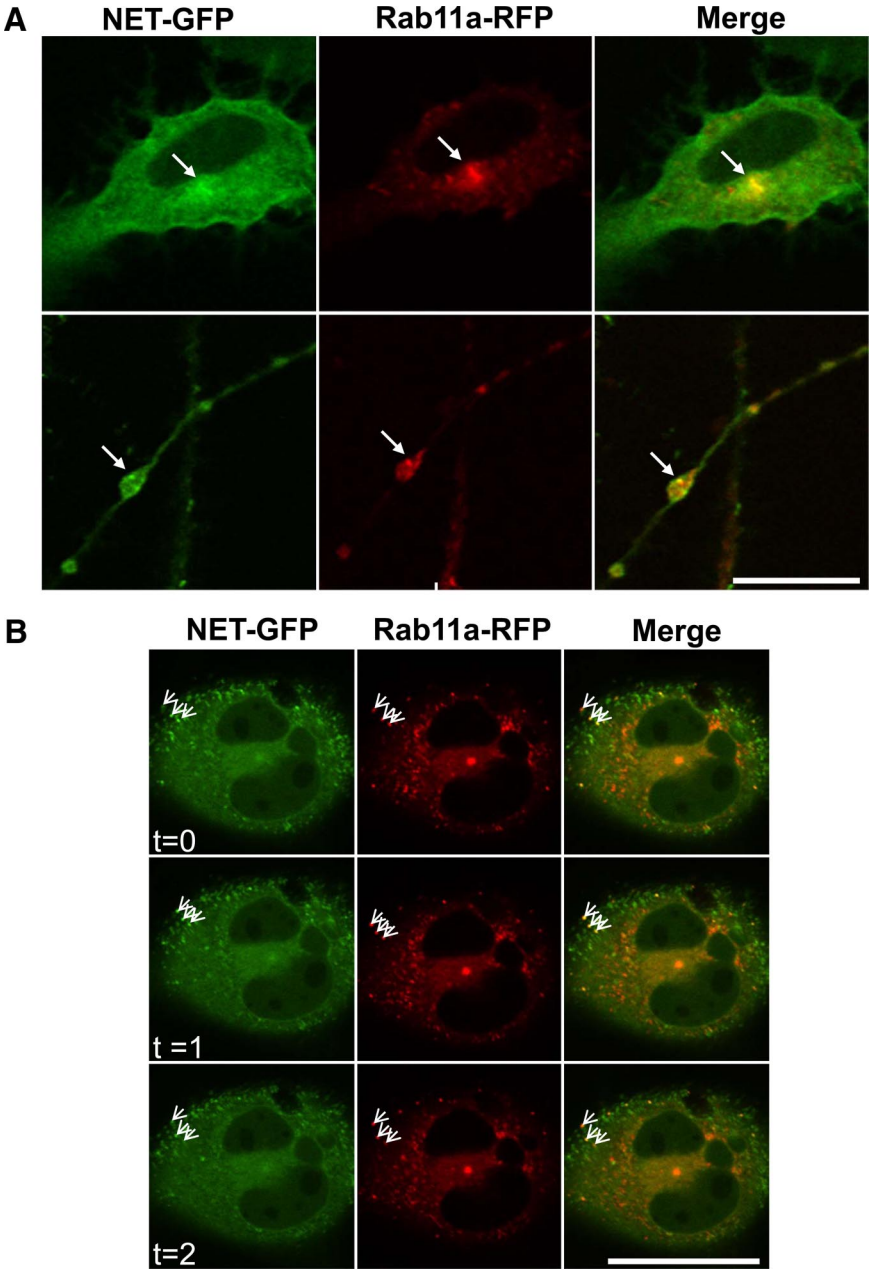

Figure 5. NET and Rab11a colocalize in living CAD cells. ***A***, GFP-NET and RFP-Rab11a were coexpressed in CAD cells. In the top row are single confocal sections of the cell bodies showing GFP-NET and RFP-Rab11a; the arrows indicate colocalization. In axonal swellings, these two fusion proteins also colocalize (second row; see arrows). Scale bar, 25 μm. ***B***, Shown are single confocal sections of cell bodies from cells expressing GFP-NET and RFP-Rab11a at three different time points, collected approximately every 35 s. The three arrows indicate examples of motile organelles in close proximity coexpressing both GFP-NET and RFP-Rab11a, in which GFP and RFP fluorescence have synchronous motility. Scale bar, 50 μm.

To determine whether Rab11a has a role in delivering NET to the recycling endosome, we asked whether GFP-NET and mCherry-FIP2ΔC2 colocalize (Fig. 6*B*). We double transfected CAD cells with vectors to induce the expression of both proteins. We found that, in swellings, the organelles containing either GFP-NET or mCherry-FIP2ΔC2 appear to have different morphologies and motile properties (Fig. 6*B*). We also observed a low level of diffuse staining for both proteins, which we interpret as the presence GFP-NET and mCherry-FIP2ΔC2 on small organelles (Fig. 6*B*). In addition, we noted larger motile fluorescent organelles containing either NET or FIP2ΔC2 that moved independently, suggesting that the majority of NET and FIP2ΔC2 are in distinct organelles (Fig. 6*B*). Occasionally, organelles with FIP2ΔC2 appeared to track the inner surface of the plasma membrane (Fig. 6*B*). Additionally, the expression of FIP2ΔC2 appeared to increase GFP-NET found at the surface of the axonal swellings (Fig. 6*B*) compared with control (Fig. 6*A*, top row).

In the cell bodies, occasionally a minor fraction of GFP-NET was observed in perinuclear, FIP2ΔC2-rich domains (Fig. 6*C*, arrow), but as in the axonal swellings, the distributions were

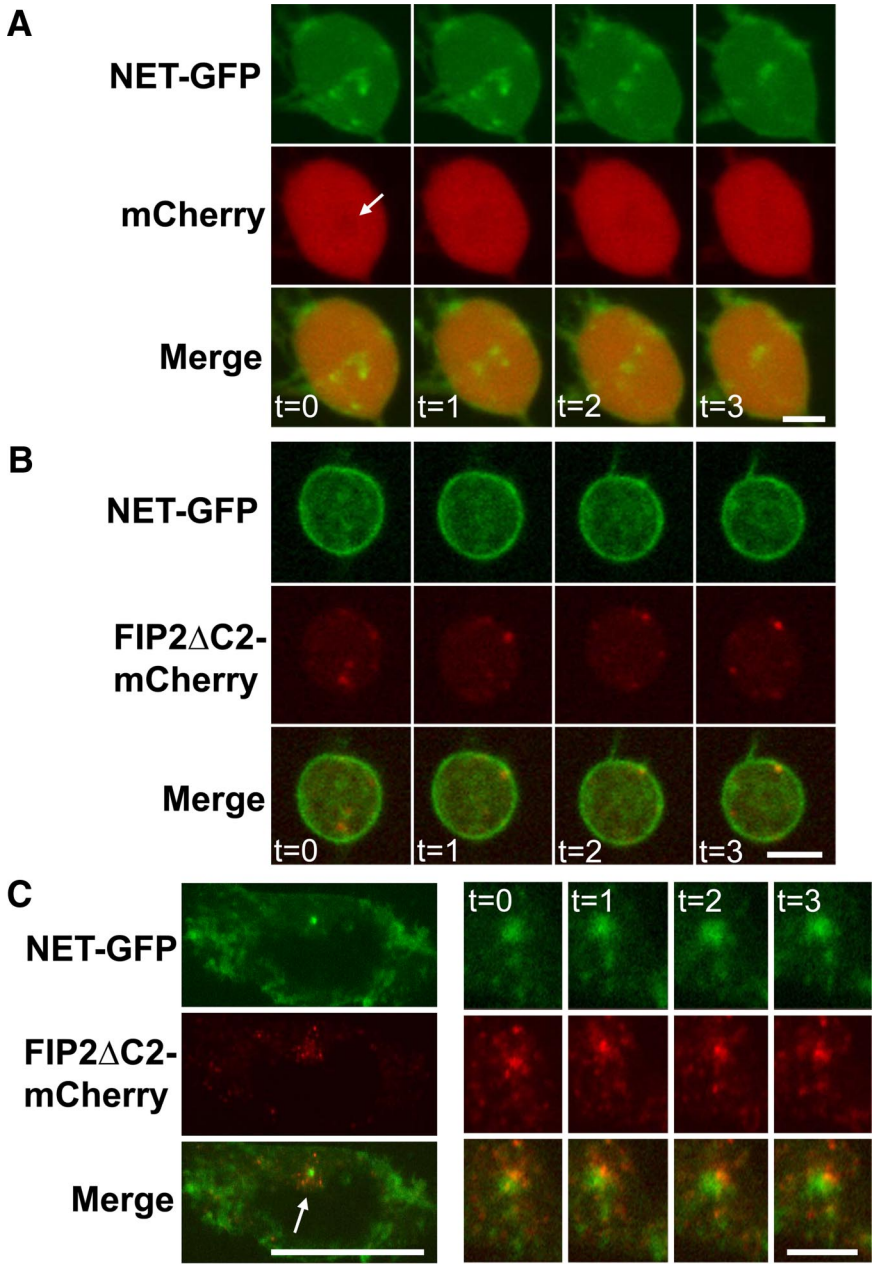

Figure 6. GFP-NET and FIP2ΔC2 do not colocalize in living CAD cells. CAD cells were transfected with both GFP-NET and either mCherry or mCherry-FIP2 C2Δ. ***A***, Shown are single confocal sections GFP-NET in axonal swellings from control cells with mCherry at four time points separated by 30 s. We observed discrete regions of dense motile GFP-NET not interacting with mCherry. ***B***, GFP-NET and mCherry-FIP2ΔC2 in axonal swellings do not colocalize, do not have similar morphologies, nor move in synchrony. Displayed are single confocal sections taken at four time points at 30 s intervals. Note that, occasionally, mCherry-FIP2ΔC2 tracks inner surface of GFP-NET demarcated perimeter. ***C***, Neither colocalization nor synchronous movements were detected in cell bodies expressing GFP-NET and mCherry-FIP2ΔC2. The majority of areas with the most intense fusion protein localization were detected in non-overlapping regions of the cell body (low-magnification confocal section of one entire cell body). However, a fraction of GFP-NET did concentrate in perinuclear regions in which a much larger fraction of mCherry-FIP2ΔC2 is detected (see arrow in merged image on the left). However, observation of these regions in time series revealed that GFP-NET and mCherry-FIP2ΔC2 do not move with similar motile properties. See images of four time points generated every 30 s on the right side. Scale bars, 5 μm.

distinct as were the motile properties (Fig. 6*C*). Together, the results from both cell bodies and boutons suggest that Rab11 is required for delivery of NET to the recycling endosome.

Coexpression of Rab11a/b mutants and NET modifies the subcellular distribution of NET

AMPH treatment leads to colocalization of NET and Rab11a-positive organelles (Figs. 1–3). Furthermore, NET is sorted to RFP-Rab11a-enriched organelles (Fig. 6) and expression of FIP2ΔC2 leads to increased cell surface NET levels and possibly prevents NET entry into recycling endosomes. FIP2 binds and therefore can sequester all Rab11 family members. This includes Rab11a, Rab11b, and the epithelial expressed Rab25 (Hales et al., 2001). However, Rab25 is not expressed in neuronal cells (Goldenring et al., 1993). Therefore, to determine whether the other two neuronal Rabs members (Rab11a/b) contribute to NET trafficking, we expressed GFP-NET with various mutants of Rab11a and Rab11b. Expression of mutants of Rab11 in a neuroendocrine cell line inhibits regulated exocytosis (Khvotchev et al., 2003). Curiously, it has been shown that Rab11 isoforms can differentially regulate the trafficking of a particular cargos despite 90% identity between Rab11a and b and can have different subcellular distributions (Khvotchev et al., 2003; Lapierre et al., 2003; Delisle et al., 2009; Silvis et al., 2009).

Therefore, we coexpressed GFP-NET with three different mutants of Rab11 in CAD cells to determine whether they colocalize and/or alter the distribution of NET in varicosities (Fig. 7). We used Rab11s with either GTP bound (S20V) or GDP bound (S25N). Also, we took advantage of another mutant that may only interact with a subset of Rab11 effectors (S29F). These proteins have previously been used to demonstrate the requirement of Rab11 in the transferrin receptor trafficking (TfnR) (Ullrich et al., 1996; Ren et al., 1998; Pasqualato et al., 2004). All mutant forms for both Rab11a and Rab11b tended to modify NET cellular distribution. Wild type, S20V, and S29F colocalize with NET in juxtamembranous organelles as well as in internal organelles (Fig. 7*A*). These results confirm our observation obtained with Rab11 SCGNs (Fig. 1). Importantly, S25N was noted to colocalize with NET predominantly in internal organelles (Fig. 7*A*). Although all mutant versions of Rab11a tended to increase colocalization with NET with respect to wild type, only Rab11a S20V reached significance (Student's *t* test, $^*p \leq 0.05$) (Fig. 7*A*,*C*). Coexpression of wild type and Rab11b mutants also led to colocalization with NET at juxtamembrane and intracellular domains. However, in contrast to Rab11a S29F, the Rab11b S29F version demonstrated significantly less colocalization with NET with respect to wild type (Student's *t* test, $^*p \leq 0.05$) (Fig. 7*B*,*C*). Rab11b S25N did not have a tendency for higher colocalization with NET compared with wild-type Rab11b, but as for Rab11a, this colocalization was predominantly on intracellular organelles. Rab11b tended to be highly enriched in varicosities but with a diffuse distribution consistent with the

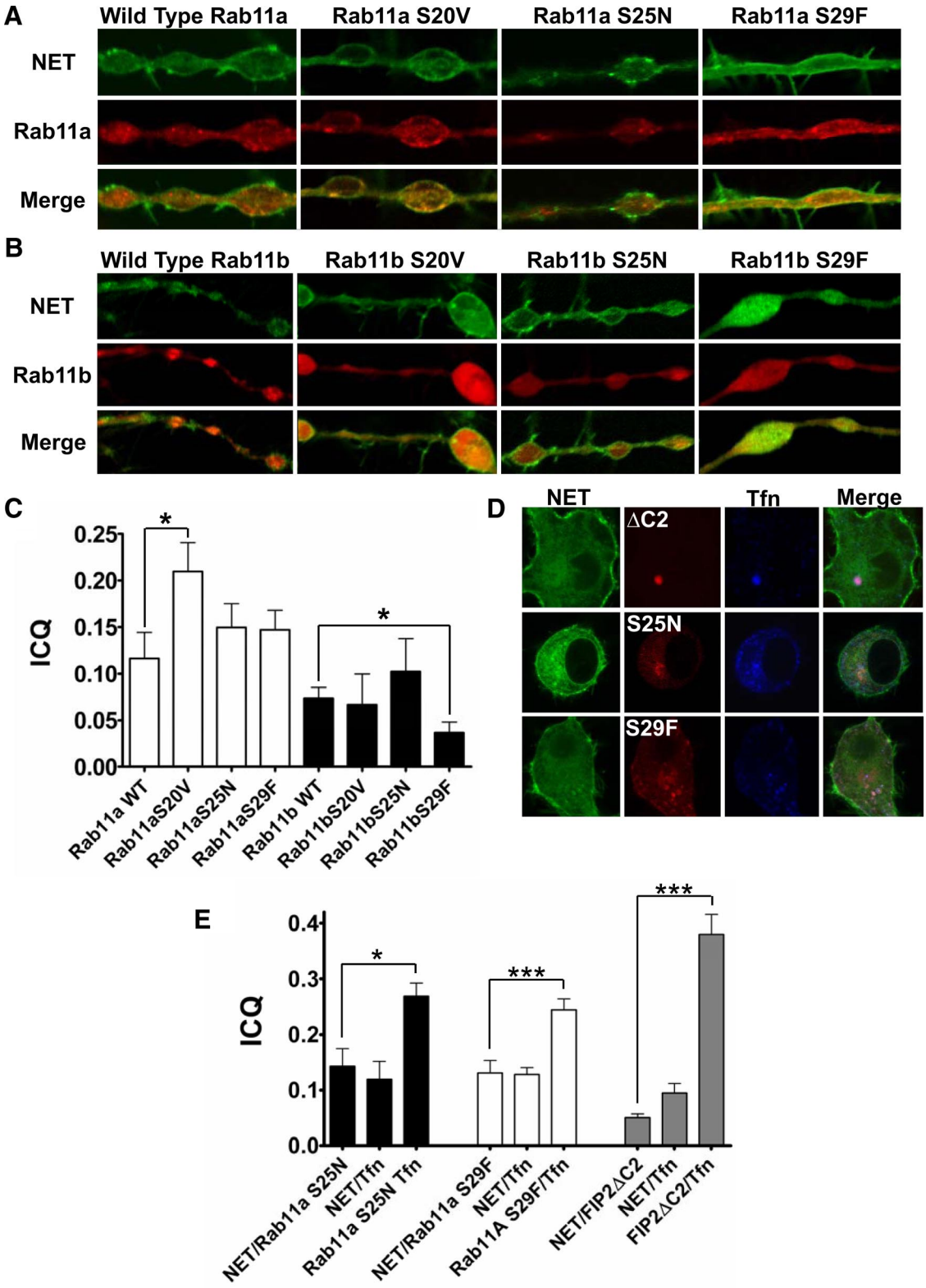

Figure 7. Mutants of Rab11a/b modify GFP-NET intracellular distribution. ***A***, NET colocalizes with various Rab11a/b mutants in boutons of CAD cells. CAD cells were transfected with both GFP-NET and various mCherry-Rab11a/b mutants. Shown are single confocal sections of axonal swellings of GFP-NET (top row) and Rab11a (middle row) and colocalization visualized in the merged images (bottom row). The mutant version is indicated above each column. ***B***, Shown are single confocal sections of axonal swellings of GFP-NET (top row) and Rab11b (middle row) and colocalization visualized in the merged images (bottom row). The mutant version is indicated above each column. ***C***, Colocalization was quantitated using the ICQ method as outlined in Materials and Methods (Li et al., 2004), demonstrating that the colocalization of NET and Rab11a/b depends on Rab11 function. ***D***, Shown are single confocal sections of cell bodies of double-transfected CAD cells with GFP-NET and the relevant mCherry-tagged protein. GFP-NET is in the first column, and Rab11 functional modifiers in the second column, Alexa 633-transferrin (Tfn) in the third column, and the triple-merged image in the last column. The name of the mutant is given to the panel of the row of the relevant images (ΔC2, mCherry-FIP2ΔC; S25N, mCherry-Rab11aS25N; S29F, mCherry-Rab11aS29F). ***E***, Colocalization was quantitated using the ICQ method as outlined in Materials and Methods (Li et al., 2004), demonstrating that the distribution of NET and Tfn differentially depend on Rab11 function. Error bars indicate SEM.

notion that it has a role in synaptic vesicle metabolism (Khvotchev et al., 2003). Expression of Rab11b generated less colocalization with NET than Rab11a. In addition, identical mutations in Rab11a/b showed different responses, suggesting that they might use different effectors to modify NET distribution. Nonetheless, these data suggest that Rab11a/b regulate NET trafficking, as mutations in these Rabs change NET/Rab11 colocalization.

In nonpolarized and polarized cells, NET responds to Rab11 mutants in a different manner than the TfnR. The TfnR exhibits a peripheral distribution and does not colocalize with Rab11a S25N, whereas it does colocalize with Rab11a S29F (Ullrich et al., 1996; Ren et al., 1998; Pasqualato et al., 2004). Furthermore, the TfnR colocalizes with FIP2ΔC2, and the sum of these experiments has led to the most accepted hypothesis that Rab11 plays a role in trafficking from the recycling endosome to the plasma membrane. Therefore, we decided to compare the distribution of NET and the TfnR in our CAD cells. We coexpressed tagged versions of NET and FIP2ΔC2, Rab11a S25N, and Rab11a S29F and allowed fluorescent transferrin (Tfn) to equilibrate with internal TfnR. Then, we determined colocalization of NET and the relevant Rab-interfering protein, NET and Tfn, and finally Rab-interfering protein and Tfn. For these studies we only used cell bodies since we only detected extremely low levels of Tfn in varicosities as expected (Cameron et al., 1991). As we determined in the varicosities, NET localized with Rab11a S25N and Rab11a S29F but not with FIP2ΔC2 (Fig. 7*D*,*E*). Tfn did colocalize with all three Rab11-interfering proteins and most strongly with FIP2ΔC2 (Fig. 7*D*,*E*). These studies suggest that Rab11 function differentially delivers cargo (e.g., NET vs Tfn) to recycling endosomes and apparently TfnR trafficking in neurons diverges somewhat from other cell types.

NET trafficking involves Rab11a function

AMPH causes NET trafficking away from the plasma membrane leading to the enrichment of NET in Rab11a compartments (Figs. 2–4). Rab11a plays a role in the trafficking of cargo from sorting endosomes to recycling endosomes and from recycling endosomes to the plasma membrane (Ullrich et al., 1996; Ren et al., 1998; Wang et al., 2000). We hypothesized that AMPH-regulated NET trafficking is supported by Rab11a. To test this hypothesis, we disrupted Rab11a function by expressing FIP2ΔC2 and then measured the consequence of this on AMPH-induced NET trafficking. First, we transfected NET cells with FIP2ΔC2 tagged with mCherry, and as expected, the majority of FIP2ΔC2 was found in a perinuclear distribution (Fig. 8*A*, top panels) (Hales et al., 2002). Next, we determined whether Rab11a is involved in AMPH-induced NET trafficking by transfecting NET cells with FIP2ΔC2 and exposing them to AMPH for up to 30 min. Figure 8*B* shows that the proportion of NET on the cell surface (biotinylated fraction) of vector-transfected NET cells noticeably decreased on 30 min AMPH treatment compared with vehicle-treated controls. AMPH did not affect the level of total NET. In contrast, expression of FIP2ΔC2 strongly reduced the ability of AMPH to cause NET internalization after 30 min (Fig. 8*B*). Quantitative analysis demonstrated that significant AMPH-induced internalization occurred in control vector-transfected cells (filled bars), whereas we observed no effect of AMPH on surface levels of NET in FIP2ΔC2-transfected cells (open bars) at 10 or 30 min of AMPH exposure (Fig. 8*C*). Data were normalized to total NET protein and expressed as percentage of the respective vehicle-treated controls (Student's *t* test, $^*p \leq 0.05$). These results

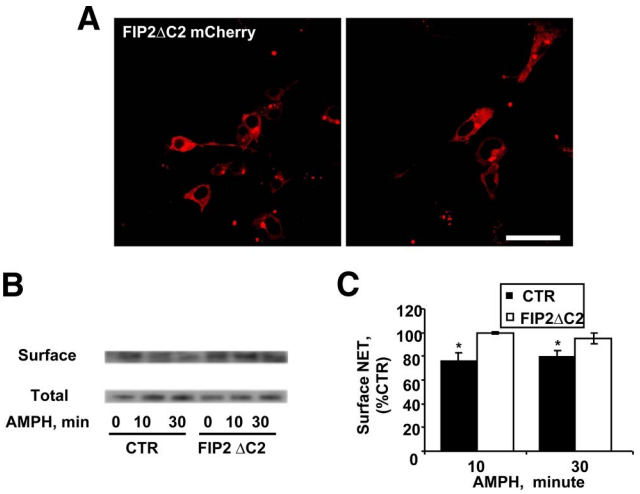

Figure 8. Expression of FIP2ΔC2 in NET cells prevents AMPH-induced internalization of NET. ***A***, FIP2ΔC2 in NET cell is found mainly in the expected perinuclear regions. Scale bar, 50 μm. ***B***, Control (CTR) (vector-transfected) and FIP2ΔC2-transfected NET cells were treated with vehicle or AMPH for 10 or 30 min, and cell surface NET was determined by biotinylation assays. Displayed is an immunoblot of biotinylated (surface NET) and total NET fractions from a representative experiment. ***C***, A graph of the quantitation of pooled data ($N = 7$) obtained from NET cells, vector (CTR)- or FIP2ΔC2-transfected, treated with vehicle or AMPH for 10 and 30 min. Data were normalized to total proteins and expressed as a percentage of control. Error bars indicate SEM.

suggest that AMPH-regulated NET trafficking requires functional Rab11a.

Rab11 and Rab4 can facilitate the delivery of vesicles to certain compartments (Zerial and McBride, 2001). Rab4 typically controls traffic from the early endosomes to the plasma membrane (van der Sluijs et al., 1992). Because NET accumulates in Rab4-positive sites with AMPH treatment (Figs. 4*A–D*, 5*A*,*B*), we suspected that NET may be returned to the cell surface through this Rab4-regulated pathway. To address this question, we disrupted Rab4 function by transiently transfecting either the GDP-locked version of the protein, Rab4 S22N (DN Rab4), or empty vector into NET cells and compared AMPH-induced internalization by cell surface biotinylation. Consistent with our previous results, both 10 and 30 min treatments with 10 μM AMPH decrease surface expression of NET in empty vector-transfected cells, whereas NET surface expression did not significantly change in cells transfected with DN Rab4 (data not shown). This result implies that AMPH-regulated NET trafficking does indeed involve both Rab11 and Rab4.

Discussion

NET is responsible for the reuptake of synaptically released NE and therefore plays an important role in regulating the fidelity of NE signaling and the maintenance of NE levels (Xu et al., 2000; Bonisch and Bruss, 2006). NE homeostasis is regulated both by modifying the NET turnover rate and the number of active NETs at the plasma membrane. Thus, it is possible that the level of functional NET is fine-tuned to the appropriate degree depending on physiological requirements. Importantly, NET trafficking may be one critical mechanism for the dynamic control of NE homeostasis. An example of altered NE homeostasis as a result of misregulation of NET surface levels is demonstrated by a polymorphism in human NET (F528C NET). This polymorphism was originally found in a screen for candidate genes associated with blood pressure homeostasis (Halushka et al., 1999) and recently linked to major depression (Haenisch et al., 2008). The

expression of F528C NET in a heterologous system displays elevated plasma membrane levels (Hahn et al., 2005). F528C NET shows reduced trafficking away from the plasma membrane in response to phorbol esters and activation of PKC (Hahn et al., 2005). In this context, it is interesting to note that PKC has been suggested to be essential for the entry of endocytosed cargo into recycling endosomes (Becker and Hannun, 2003) and that F528C NET has been linked to brain disorders (Haenisch et al., 2008). Another important aspect of NET trafficking is that NET has been linked to the actions of psychostimulants such as AMPH. AMPH decreases NET plasma membrane expression and affects NE homeostasis, possibly leading to vasculitis, neuropsychiatric abnormalities, and cardiomyopathy (Furst et al., 1990; Varner et al., 2002; Pozzi et al., 2008). One possibility is that AMPH reduces NET surface expression by shifting a portion of NETs into a recycling endosomal compartment. Therefore, it is imperative to understand the molecular underpinnings of the regulation of NET trafficking and whether the recycling endosome is involved in this process. Here, our intent is to further clarify the mechanisms and membrane compartments used by AMPH to alter NE homeostasis.

The main goals of this study were to determine whether AMPH treatment leads to NET internalization in neurons and single boutons, whether this internalization is via Rab11 or Rab4 compartments, and whether this internalization requires Rab11 function. We chose to perform these experiments using (1) brain slices, allowing us to determine whether AMPH modifies NET surface levels in the context of CNS circuitry; (2) SCGNs, permitting single-bouton analysis; and (3) a catecholaminergic neuronal cell line useful for genetic manipulation and biochemistry. We found that AMPH does promote a reduction in surface NET in cortical brain slices, indicating that AMPH can reduce neuronal NET in a "native" environment (Fig. 1). AMPH treatment also led to an intracellular accumulation of NET and sorting of NET to Rab11- and Rab4-positive compartments (Figs. 1–3). Blocking Rab11 function with a truncated Rab11 binding protein (FIP2ΔC2) led to apparent elevation of NET on the plasma membrane, prevented entry of NET to recycling endosomes, and prevented AMPH-induced internalization (Figs. 6, 8). Trapping Rab11a/b in either the GDP or GTP state by using the Rab11 S20V and S25N mutants, respectively, altered NET trafficking as does a mutation (S29F), which modifies the ability of Rab11 to traffic cargo in the usual manner (Pasqualato et al., 2004). This mutant alters the distribution of an early endosome marker, as does FIP2ΔC2 (Hales et al., 2002; Pasqualato et al., 2004). Rab11 and Rab4 also colocalize on a subset of endosomes (Sönnichsen et al., 2000), and recently a protein (D-AKAP/AKAP10) binding both Rab4 and Rab11 has been identified (Eggers et al., 2009). In this context, we suggest that Rab11 facilitates NET entry into recycling endosomes.

Under basal conditions, at the level of synaptic boutons, we observed Rab11a and interacting proteins just below the plasma membrane and on internal organelles with modest colocalization of NET and Rab11a (Fig. 1). At early time points after AMPH treatment (10 min), we noticed potential sites of clathrin assembly in domains adjacent to the NET-enriched domains (Fig. 4). Based on our previous work, these domains may be lipid rafts (Matthies et al., 2009). Curiously, juxtaplasma membrane Rab11a tended to be detected at sites of clathrin enrichment (Fig. 4). In the interior of the bouton, clathrin also appeared to accumulate on internal organelles, and again Rab11a was detected at these sites (Fig. 4). Importantly, at early time points, NET appeared to be in a diffuse intrabouton pattern (Fig. 4), and after sustained activation of endocytosis by AMPH, we detected NET in larger Rab11a-positive organelles (Fig. 1). Our gradient analysis of NET redistribution uncovered that NET internalization occurs predominantly from a subset plasma membrane fractions with a rather low density. Based on our previous study, we suggest NET is initially found in lipid rafts (Matthies et al., 2009). Therefore, it is possible that the low-density plasma membrane fraction that showed preferential AMPH-induced NET loss is enriched for lipid rafts. During the earliest time points of this process, Rab11a may intersect with the NET endocytic cycle at the clathrin-coated pit stage. This stage occurs in nonlipid raft domains as opposed to clathrin-independent endocytosis as discussed by Donaldson et al. (2009). In support of this hypothesis, purified clathrin-coated vesicles contain Rab11a (Blondeau et al., 2004; Borner et al., 2006), suggesting that Rab11a might remain on endocytic vesicles containing NET.

In these studies, we demonstrated that AMPH-induced (30 min) NET delivery to recycling endosomes requires Rab11 function (Fig. 8). The main consequence of suppressing Rab11 function by FIP2ΔC2 is that NET entry into recycling endosomes is modified. Expression of FIP2ΔC2 leads to its accumulation with Rab11 and myosin at the recycling endosome (Hales et al., 2002; Lindsay and McCaffrey, 2002, 2004; Fan et al., 2004). We speculate that the level of available, non-mislocalized Rab11 is below a threshold, and therefore, NET fails to be delivered to the recycling endosome. Thus, the expression of FIP2ΔC2 might increase NET plasma membrane expression, as under these conditions, the fraction of NET normally entering the endosome recycling system now localizes to the plasma membrane. This might explain why the expression of FIP2ΔC2 inhibits AMPH-induced trafficking. This role for Rab11 has been previously suggested for other endocytosed membrane proteins (Ullrich et al., 1996; Ren et al., 1998). Consistent with this hypothesis, knockdown of several Rab11 effectors leads to observations that strengthen this novel role of Rab11 (Schwenk et al., 2007; Welsh et al., 2007; Schonteich et al., 2008; Eggers et al., 2009). Indeed, knockdown of Rab11FIP5 leads to faster recycling and higher cell surface expression of membrane proteins (Schonteich et al., 2008). Similar results were obtained by knocking down a recently identified effector (D-AKAP2/AKAP10) of both Rab4 and Rab11 protein (Eggers et al., 2009). Finally, knockdown of Rab11FIP2 and FIP5 leads to increased cell surface levels of the glucose transporter (GLUT4) (Schwenk et al., 2007; Welsh et al., 2007; Schonteich et al., 2008; Eggers et al., 2009).

To further probe the role of Rab11 in NET trafficking by an alternative approach, we tested the effects of several mutants of Rab11a/b on NET trafficking. These mutants alter the preferred bound nucleotide acting as constitutively active (S20V) or dominant-negative mutant (S25N). Analysis of NET distribution in cells expressing these mutants also point to the hypothesis that Rab11a/b has a role in delivering NET under basal conditions to recycling endosomes (Fig. 7). We also tested a Rab11 mutant (S29F) that alters the distribution of early endosome markers as does FIP2ΔC2 (Hales et al., 2002; Pasqualato et al., 2004). These mutants affect the basal distribution of NET (Fig. 7). These data also point out a differential regulation of NET basal trafficking by Rab11a and Rab11b (Fig. 7). Curiously, knockdown of Rab11FIP and D-AKAP2/AKAP10 also alters the distribution of early endosome markers, as well as increases cell surface expression of membrane proteins (Schwenk et al., 2007; Welsh et al., 2007; Schonteich et al., 2008; Eggers et al., 2009).

Unlike NET, TfnR trafficking has been shown not to be affected by AMPH (Boudanova et al., 2008). Consistent with these

observations, expression of FIP2ΔC2, Rab1a S25N, and Rab11a S29F differentially affects TfnR and NET trafficking. This implies that NET uses a pathway that is either not used by TfnR or TfnR trafficking can use alternative pathways to get to the endosomal recycling compartment particularly in the presence of FIP2ΔC2.

NET and Rab4 colocalize on a subset of endosomes on AMPH treatment. However, expression of a GDP-locked version of Rab4 inhibits AMPH-induced intracellular accumulation of NET. Although this is surprising, Zadeh et al. (2008) have shown that the Kv1.5 channel increases plasma membrane levels when a dominant-negative Rab4 mutant is expressed. Consistent with our new role of Rab4 in NET trafficking, it has been shown that GLUT4 and the serotonin transporter also do not respond as predicted by the standard Rab4 model to Rab4 mutant expression (Cormont et al., 1996; Ahmed et al., 2008).

Rab11 and Rab4 colocalize on a subset of endosomes (Sönnichsen et al., 2000). In this context, another possibility is that Rab11 can facilitate NET entry into the recycling endosomes, possibly in concert with Rab4 (Eggers et al., 2009). This would be consistent with observations that perturbations of Rab11 function can lead to changes in the distribution of the early endosome Rab5 effector EEA1 (Hales et al., 2001; Pasqualato et al., 2004; Schwenk et al., 2007; Welsh et al., 2007; Schonteich et al., 2008; Eggers et al., 2009).

These studies demonstrate for the first time AMPH-induced trafficking of a neurotransmitter transporter within a native brain environment and in a single bouton and show that both Rab11a/b and Rab4 regulate NET trafficking. These results suggest that these Rabs may thus be involved in modulating NE homeostasis.

References

Ahmed BA, Jeffus BC, Bukhari SI, Harney JT, Unal R, Lupashin VV, van der Sluijs P, Kilic F (2008) Serotonin transamidates Rab4 and facilitates its binding to the C terminus of serotonin transporter. J Biol Chem 283:9388–9398.

Apparsundaram S, Galli A, DeFelice LJ, Hartzell HC, Blakely RD (1998a) Acute regulation of norepinephrine transport: I. Protein kinase C-linked muscarinic receptors influence transport capacity and transporter density in SK-N-SH cells. J Pharmacol Exp Ther 287:733–743.

Apparsundaram S, Schroeter S, Giovanetti E, Blakely RD (1998b) Acute regulation of norepinephrine transport: II. PKC-modulated surface expression of human norepinephrine transporter proteins. J Pharmacol Exp Ther 287:744–751.

Bauman AL, Apparsundaram S, Ramamoorthy S, Wadzinski BE, Vaughan RA, Blakely RD (2000) Cocaine and antidepressant-sensitive biogenic amine transporters exist in regulated complexes with protein phosphatase 2A. J Neurosci 20:7571–7578.

Becker KP, Hannun YA (2003) cPKC-dependent sequestration of membrane-recycling components in a subset of recycling endosomes. J Biol Chem 278:52747–52754.

Billington D, Maltby PJ, Jackson AP, Graham JM (1998) Dissection of hepatic receptor-mediated endocytic pathways using self-generated gradients of iodixanol (OptiPrep). Anal Biochem 258:251–258.

Blondeau F, Ritter B, Allaire PD, Wasiak S, Girard M, Hussain NK, Angers A, Legendre-Guillemin V, Roy L, Boismenu D, Kearney RE, Bell AW, Bergeron JJ, McPherson PS (2004) Tandem MS analysis of brain clathrin-coated vesicles reveals their critical involvement in synaptic vesicle recycling. Proc Natl Acad Sci U S A 101:3833–3838.

Bohn LM, Xu F, Gainetdinov RR, Caron MG (2000) Potentiated opioid analgesia in norepinephrine transporter knock-out mice. J Neurosci 20:9040–9045.

Bonisch H, Bruss M (2006) The norepinephrine transporter in physiology and disease. Handb Exp Pharmacol 485–524.

Borner GH, Harbour M, Hester S, Lilley KS, Robinson MS (2006) Comparative proteomics of clathrin-coated vesicles. J Cell Biol 175:571–578.

Boudanova E, Navaroli DM, Melikian HE (2008) Amphetamine-induced decreases in dopamine transporter surface expression are protein kinase C-independent. Neuropharmacology 54:605–612.

Cameron PL, Südhof TC, Jahn R, De Camilli P (1991) Colocalization of synaptophysin with transferrin receptors: implications for synaptic vesicle biogenesis. J Cell Biol 115:151–164.

Chamberlain LH, Burgoyne RD, Gould GW (2001) SNARE proteins are highly enriched in lipid rafts in PC12 cells: implications for the spatial control of exocytosis. Proc Natl Acad Sci U S A 98:5619–5624.

Collins MO, Yu L, Coba MP, Husi H, Campuzano I, Blackstock WP, Choudhary JS, Grant SG (2005) Proteomic analysis of in vivo phosphorylated synaptic proteins. J Biol Chem 280:5972–5982.

Collins MO, Yu L, Campuzano I, Grant SG, Choudhary JS (2008) Phosphoproteomic analysis of the mouse brain cytosol reveals a predominance of protein phosphorylation in regions of intrinsic sequence disorder. Mol Cell Proteomics 7:1331–1348.

Cormont M, Bortoluzzi MN, Gautier N, Mari M, van Obberghen E, Le Marchand-Brustel Y (1996) Potential role of Rab4 in the regulation of subcellular localization of Glut4 in adipocytes. Mol Cell Biol 16:6879–6886.

Delisle BP, Underkofler HA, Moungey BM, Slind JK, Kilby JA, Best JM, Foell JD, Balijepalli RC, Kamp TJ, January CT (2009) Small GTPase determinants for the Golgi processing and plasmalemmal expression of human ether-a-go-go related (hERG) K^+ channels. J Biol Chem 284:2844–2853.

Dipace C, Sung U, Binda F, Blakely RD, Galli A (2007) Amphetamine induces a calcium/calmodulin-dependent protein kinase II-dependent reduction in norepinephrine transporter surface expression linked to changes in syntaxin 1A/transporter complexes. Mol Pharmacol 71:230–239.

Donaldson JG, Porat-Shliom N, Cohen LA (2009) Clathrin-independent endocytosis: a unique platform for cell signaling and PM remodeling. Cell Signal 21:1–6.

Eggers CT, Schafer JC, Goldenring JR, Taylor SS (2009) D-AKAP2 interacts with Rab4 and Rab11 through its RGS domains and regulates transferrin receptor recycling. J Biol Chem 284:32869–32880.

Esler M, Alvarenga M, Pier C, Richards J, El-Osta A, Barton D, Haikerwal D, Kaye D, Schlaich M, Guo L, Jennings G, Socratous F, Lambert G (2006) The neuronal noradrenaline transporter, anxiety and cardiovascular disease. J Psychopharmacol 20:60–66.

Fan GH, Lapierre LA, Goldenring JR, Sai J, Richmond A (2004) Rab11-family interacting protein 2 and myosin Vb are required for CXCR2 recycling and receptor-mediated chemotaxis. Mol Biol Cell 15:2456–2469.

Ford T, Graham J, Rickwood D (1994) Iodixanol: a nonionic iso-osmotic centrifugation medium for the formation of self-generated gradients. Anal Biochem 220:360–366.

Furst SR, Fallon SP, Reznik GN, Shah PK (1990) Myocardial infarction after inhalation of methamphetamine. N Engl J Med 323:1147–1148.

Garcia BG, Wei Y, Moron JA, Lin RZ, Javitch JA, Galli A (2005) Akt is essential for insulin modulation of amphetamine-induced human dopamine transporter cell-surface redistribution. Mol Pharmacol 68:102–109.

Goldenring JR, Shen KR, Vaughan HD, Modlin IM (1993) Identification of a small GTP-binding protein, Rab25, expressed in the gastrointestinal mucosa, kidney, and lung. J Biol Chem 268:18419–18422.

Graham JM (2001) Isolation of Golgi membranes from tissues and cells by differential and density gradient centrifugation. Curr Protoc Cell Biol 3:3.9.

Graham J, Ford T, Rickwood D (1994) The preparation of subcellular organelles from mouse liver in self-generated gradients of iodixanol. Anal Biochem 220:367–373.

Grosshans BL, Ortiz D, Novick P (2006) Rabs and their effectors: achieving specificity in membrane traffic. Proc Natl Acad Sci U S A 103:11821–11827.

Haenisch B, Linsel K, Brüss M, Gilsbach R, Propping P, Nöthen MM, Rietschel M, Fimmers R, Maier W, Zobel A, Höfels S, Guttenthaler V, Göthert M, Bönisch H (2008) Association of major depression with rare functional variants in norepinephrine transporter and serotonin(1A) receptor genes. Am J Med Genet B Neuropsychiatr Genet 150B:1013–1016.

Hahn MK, Blakely RD (2002) Monoamine transporter gene structure and polymorphisms in relation to psychiatric and other complex disorders. Pharmacogenomics J 2:217–235.

Hahn MK, Robertson D, Blakely RD (2003) A mutation in the human norepinephrine transporter gene (SLC6A2) associated with orthostatic intolerance disrupts surface expression of mutant and wild-type transporters. J Neurosci 23:4470–4478.

Hahn MK, Mazei-Robison MS, Blakely RD (2005) Single nucleotide polymorphisms in the human norepinephrine transporter gene affect expression, trafficking, antidepressant interaction, and protein kinase C regulation. Mol Pharmacol 68:457–466.

Hahn MK, Blackford JU, Haman K, Mazei-Robison M, English BA, Prasad HC, Steele A, Hazelwood L, Fentress HM, Myers R, Blakely RD, Sanders-Bush E, Shelton R (2008) Multivariate permutation analysis associates multiple polymorphisms with subphenotypes of major depression. Genes Brain Behav 7:487–495.

Hales CM, Griner R, Hobdy-Henderson KC, Dorn MC, Hardy D, Kumar R, Navarre J, Chan EK, Lapierre LA, Goldenring JR (2001) Identification and characterization of a family of Rab11-interacting proteins. J Biol Chem 276:39067–39075.

Hales CM, Vaerman JP, Goldenring JR (2002) Rab11 family interacting protein 2 associates with Myosin Vb and regulates plasma membrane recycling. J Biol Chem 277:50415–50421.

Haller J, Bakos N, Rodriguiz RM, Caron MG, Wetsel WC, Liposits Z (2002) Behavioral responses to social stress in noradrenaline transporter knockout mice: effects on social behavior and depression. Brain Res Bull 58:279–284.

Halushka MK, Fan JB, Bentley K, Hsie L, Shen N, Weder A, Cooper R, Lipshutz R, Chakravarti A (1999) Patterns of single-nucleotide polymorphisms in candidate genes for blood-pressure homeostasis. Nat Genet 22:239–247.

Hashiramoto M, James DE (2000) Characterization of insulin-responsive GLUT4 storage vesicles isolated from 3T3-L1 adipocytes. Mol Cell Biol 20:416–427.

Herman GA, Bonzelius F, Cieutat AM, Kelly RB (1994) A distinct class of intracellular storage vesicles, identified by expression of the glucose transporter GLUT4. Proc Natl Acad Sci U S A 91:12750–12754.

Iversen LL (1971) Role of transmitter uptake mechanisms in synaptic neurotransmission. Br J Pharmacol 41:571–591.

Jafar-Nejad H, Andrews HK, Acar M, Bayat V, Wirtz-Peitz F, Mehta SQ, Knoblich JA, Bellen HJ (2005) Sec15, a component of the exocyst, promotes notch signaling during the asymmetric division of *Drosophila* sensory organ precursors. Dev Cell 9:351–363.

Jordens I, Marsman M, Kuijl C, Neefjes J (2005) Rab proteins, connecting transport and vesicle fusion. Traffic 6:1070–1077.

Kaminski RM, Shippenberg TS, Witkin JM, Rocha BA (2005) Genetic deletion of the norepinephrine transporter decreases vulnerability to seizures. Neurosci Lett 382:51–55.

Keller NR, Robertson D (2006) Familial orthostatic tachycardia. Curr Opin Cardiol 21:173–179.

Keller NR, Diedrich A, Appalsamy M, Tuntrakool S, Lonce S, Finney C, Caron MG, Robertson D (2004) Norepinephrine transporter-deficient mice exhibit excessive tachycardia and elevated blood pressure with wakefulness and activity. Circulation 110:1191–1196.

Khvotchev MV, Ren M, Takamori S, Jahn R, Südhof TC (2003) Divergent functions of neuronal Rab11b in Ca^{2+}-regulated versus constitutive exocytosis. J Neurosci 23:10531–10539.

Kim CH, Hahn MK, Joung Y, Anderson SL, Steele AH, Mazei-Robinson MS, Gizer I, Teicher MH, Cohen BM, Robertson D, Waldman ID, Blakely RD, Kim KS (2006) A polymorphism in the norepinephrine transporter gene alters promoter activity and is associated with attention-deficit hyperactivity disorder. Proc Natl Acad Sci U S A 103:19164–19169.

Kippenberger AG, Palmer DJ, Comer AM, Lipski J, Burton LD, Christie DL (1999) Localization of the noradrenaline transporter in rat adrenal medulla and PC12 cells: evidence for its association with secretory granules in PC12 cells. J Neurochem 73:1024–1032.

Klimek V, Stockmeier C, Overholser J, Meltzer HY, Kalka S, Dilley G, Ordway GA (1997) Reduced levels of norepinephrine transporters in the locus coeruleus in major depression. J Neurosci 17:8451–8458.

Lang T, Bruns D, Wenzel D, Riedel D, Holroyd P, Thiele C, Jahn R (2001) SNAREs are concentrated in cholesterol-dependent clusters that define docking and fusion sites for exocytosis. EMBO J 20:2202–2213.

Langevin J, Morgan MJ, Sibarita JB, Aresta S, Murthy M, Schwarz T, Camonis J, Bellaïche Y (2005) *Drosophila* exocyst components Sec5, Sec6, and Sec15 regulate DE-Cadherin trafficking from recycling endosomes to the plasma membrane. Dev Cell 9:365–376.

Lapierre LA, Kumar R, Hales CM, Navarre J, Bhartur SG, Burnette JO, Provance DW Jr, Mercer JA, Bähler M, Goldenring JR (2001) Myosin Vb is associated with plasma membrane recycling systems. Mol Biol Cell 12:1843–1857.

Lapierre LA, Dorn MC, Zimmerman CF, Navarre J, Burnette JO, Goldenring JR (2003) Rab11b resides in a vesicular compartment distinct from Rab11a in parietal cells and other epithelial cells. Exp Cell Res 290:322–331.

Leitner B, Lovisetti-Scamihorn P, Heilmann J, Striessnig J, Blakely RD, Eiden LE, Winkler H (1999) Subcellular localization of chromogranins, calcium channels, amine carriers, and proteins of the exocytotic machinery in bovine splenic nerve. J Neurochem 72:1110–1116.

Li Q, Lau A, Morris TJ, Guo L, Fordyce CB, Stanley EF (2004) A syntaxin 1, $G\alpha_o$, and N-type calcium channel complex at a presynaptic nerve terminal: analysis by quantitative immunocolocalization. J Neurosci 24:4070–4081.

Lim JE, Jin O, Bennett C, Morgan K, Wang F, Trenor CC 3rd, Fleming MD, Andrews NC (2005) A mutation in Sec15l1 causes anemia in hemoglobin deficit (hbd) mice. Nat Genet 37:1270–1273.

Lim SN, Bonzelius F, Low SH, Wille H, Weimbs T, Herman GA (2001) Identification of discrete classes of endosome-derived small vesicles as a major cellular pool for recycling membrane proteins. Mol Biol Cell 12:981–995.

Lindsay AJ, McCaffrey MW (2002) Rab11-FIP2 functions in transferrin recycling and associates with endosomal membranes via its COOH-terminal domain. J Biol Chem 277:27193–27199.

Lindsay AJ, McCaffrey MW (2004) The C2 domains of the class I Rab11 family of interacting proteins target recycling vesicles to the plasma membrane. J Cell Sci 117:4365–4375.

Mandela P, Ordway GA (2006) The norepinephrine transporter and its regulation. J Neurochem 97:310–333.

Matthies HJ, Han Q, Shields A, Wright J, Moore JL, Winder DG, Galli A, Blakely RD (2009) Subcellular localization of the antidepressant-sensitive norepinephrine transporter. BMC Neurosci 10:65.

Maxfield FR, McGraw TE (2004) Endocytic recycling. Nat Rev Mol Cell Biol 5:121–132.

Mellman I (1996) Endocytosis and molecular sorting. Annu Rev Cell Dev Biol 12:575–625.

Miner LH, Schroeter S, Blakely RD, Sesack SR (2003) Ultrastructural localization of the norepinephrine transporter in superficial and deep layers of the rat prelimbic prefrontal cortex and its spatial relationship to probable dopamine terminals. J Comp Neurol 466:478–494.

Miner LH, Jedema HP, Moore FW, Blakely RD, Grace AA, Sesack SR (2006) Chronic stress increases the plasmalemmal distribution of the norepinephrine transporter and the coexpression of tyrosine hydroxylase in norepinephrine axons in the prefrontal cortex. J Neurosci 26:1571–1578.

Mukherjee S, Ghosh RN, Maxfield FR (1997) Endocytosis. Physiol Rev 77:759–803.

Novick P, Zerial M (1997) The diversity of Rab proteins in vesicle transport. Curr Opin Cell Biol 9:496–504.

Oztan A, Silvis M, Weisz OA, Bradbury NA, Hsu SC, Goldenring JR, Yeaman C, Apodaca G (2007) Exocyst requirement for endocytic traffic directed toward the apical and basolateral poles of polarized MDCK cells. Mol Biol Cell 18:3978–3992.

Pacholczyk T, Blakely RD, Amara SG (1991) Expression cloning of a cocaine- and antidepressant-sensitive human noradrenaline transporter. Nature 350:350–354.

Pagano A, Crottet P, Prescianotto-Baschong C, Spiess M (2004) In vitro formation of recycling vesicles from endosomes requires adaptor protein-1/clathrin and is regulated by Rab4 and the connector Rabaptin-5. Mol Biol Cell 15:4990–5000.

Pasqualato S, Senic-Matuglia F, Renault L, Goud B, Salamero J, Cherfils J (2004) The structural GDP/GTP cycle of Rab11 reveals a novel interface involved in the dynamics of recycling endosomes. J Biol Chem 279:11480–11488.

Pozzi M, Roccatagliata D, Sterzi R (2008) Drug abuse and intracranial hemorrhage. Neurol Sci 29 [Suppl 2]:S269–S270.

Prekeris R, Klumperman J, Scheller RH (2000) A Rab11/Rip11 protein complex regulates apical membrane trafficking via recycling endosomes. Mol Cell 6:1437–1448.

Proikas-Cezanne T, Gaugel A, Frickey T, Nordheim A (2006) Rab14 is part of the early endosomal clathrin-coated TGN microdomain. FEBS Lett 580:5241–5246.

Qi Y, Wang JK, McMillian M, Chikaraishi DM (1997) Characterization of a

CNS cell line, CAD, in which morphological differentiation is initiated by serum deprivation. J Neurosci 17:1217–1225.

Ren M, Xu G, Zeng J, De Lemos-Chiarandini C, Adesnik M, Sabatini DD (1998) Hydrolysis of GTP on rab11 is required for the direct delivery of transferrin from the pericentriolar recycling compartment to the cell surface but not from sorting endosomes. Proc Natl Acad Sci U S A 95:6187–6192.

Robinson MS, Watts C, Zerial M (1996) Membrane dynamics in endocytosis. Cell 84:13–21.

Roos J, Kelly RB (1999) The endocytic machinery in nerve terminals surrounds sites of exocytosis. Curr Biol 9:1411–1414.

Rumantir MS, Kaye DM, Jennings GL, Vaz M, Hastings JA, Esler MD (2000) Phenotypic evidence of faulty neuronal norepinephrine reuptake in essential hypertension. Hypertension 36:824–829.

Savchenko V, Sung U, Blakely RD (2003) Cell surface trafficking of the antidepressant-sensitive norepinephrine transporter revealed with an ectodomain antibody. Mol Cell Neurosci 24:1131–1150.

Savina A, Fader CM, Damiani MT, Colombo MI (2005) Rab11 promotes docking and fusion of multivesicular bodies in a calcium-dependent manner. Traffic 6:131–143.

Schonteich E, Wilson GM, Burden J, Hopkins CR, Anderson K, Goldenring JR, Prekeris R (2008) The Rip11/Rab11-FIP5 and kinesin II complex regulates endocytic protein recycling. J Cell Sci 121:3824–3833.

Schroeter S, Apparsundaram S, Wiley RG, Miner LH, Sesack SR, Blakely RD (2000) Immunolocalization of the cocaine- and antidepressant-sensitive l-norepinephrine transporter. J Comp Neurol 420:211–232.

Schwenk RW, Luiken JJ, Eckel J (2007) FIP2 and Rip11 specify Rab11a-mediated cellular distribution of GLUT4 and FAT/CD36 in H9c2-hIR cells. Biochem Biophys Res Commun 363:119–125.

Shannon JR, Flattem NL, Jordan J, Jacob G, Black BK, Biaggioni I, Blakely RD, Robertson D (2000) Orthostatic intolerance and tachycardia associated with norepinephrine-transporter deficiency. N Engl J Med 342:541–549.

Sheehan D, Ray GS, Calhoun BC, Goldenring JR (1996) A somatodendritic distribution of Rab11 in rabbit brain neurons. Neuroreport 7:1297–1300.

Sheff DR, Daro EA, Hull M, Mellman I (1999) The receptor recycling pathway contains two distinct populations of early endosomes with different sorting functions. J Cell Biol 145:123–139.

Silvis MR, Bertrand CA, Ameen N, Golin-Bisello F, Butterworth MB, Frizzell RA, Bradbury NA (2009) Rab11b regulates the apical recycling of the cystic fibrosis transmembrane conductance regulator in polarized intestinal epithelial cells. Mol Biol Cell 20:2337–2350.

Somsel Rodman J, Wandinger-Ness A (2000) Rab GTPases coordinate endocytosis. J Cell Sci 113:183–192.

Sönnichsen B, De Renzis S, Nielsen E, Rietdorf J, Zerial M (2000) Distinct membrane domains on endosomes in the recycling pathway visualized by multicolor imaging of Rab4, Rab5, and Rab11. J Cell Biol 149:901–914.

Sung U, Apparsundaram S, Galli A, Kahlig KM, Savchenko V, Schroeter S, Quick MW, Blakely RD (2003) A regulated interaction of syntaxin 1A with the antidepressant-sensitive norepinephrine transporter establishes catecholamine clearance capacity. J Neurosci 23:1697–1709.

Sung U, Jennings JL, Link AJ, Blakely RD (2005) Proteomic analysis of human norepinephrine transporter complexes reveals associations with protein phosphatase 2A anchoring subunit and 14-3-3 proteins. Biochem Biophys Res Commun 333:671–678.

Torres GE, Yao WD, Mohn AR, Quan H, Kim KM, Levey AI, Staudinger J, Caron MG (2001) Functional interaction between monoamine plasma membrane transporters and the synaptic PDZ domain-containing protein PICK1. Neuron 30:121–134.

Uchida J, Kiuchi Y, Ohno M, Yura A, Oguchi K (1998) Ca^{2+}-dependent enhancement of [^{3}H]noradrenaline uptake in PC12 cells through calmodulin-dependent kinases. Brain Res 809:155–164.

Ullrich O, Reinsch S, Urbé S, Zerial M, Parton RG (1996) Rab11 regulates recycling through the pericentriolar recycling endosome. J Cell Biol 135:913–924.

van Dam EM, Stoorvogel W (2002) Dynamin-dependent transferrin receptor recycling by endosome-derived clathrin-coated vesicles. Mol Biol Cell 13:169–182.

van Dam EM, Ten Broeke T, Jansen K, Spijkers P, Stoorvogel W (2002) Endocytosed transferrin receptors recycle via distinct dynamin and phosphatidylinositol 3-kinase-dependent pathways. J Biol Chem 277:48876–48883.

van der Sluijs P, Hull M, Webster P, Måle P, Goud B, Mellman I (1992) The small GTP-binding protein rab4 controls an early sorting event on the endocytic pathway. Cell 70:729–740.

Varner KJ, Ogden BA, Delcarpio J, Meleg-Smith S (2002) Cardiovascular responses elicited by the "binge" administration of methamphetamine. J Pharmacol Exp Ther 301:152–159.

Wang X, Kumar R, Navarre J, Casanova JE, Goldenring JR (2000) Regulation of vesicle trafficking in Madin-Darby canine kidney cells by Rab11a and Rab25. J Biol Chem 275:29138–29146.

Welsh GI, Leney SE, Lloyd-Lewis B, Wherlock M, Lindsay AJ, McCaffrey MW, Tavaré JM (2007) Rip11 is a Rab11- and AS160-RabGAP-binding protein required for insulin-stimulated glucose uptake in adipocytes. J Cell Sci 120:4197–4208.

Wersinger C, Jeannotte A, Sidhu A (2006) Attenuation of the norepinephrine transporter activity and trafficking via interactions with alpha-synuclein. Eur J Neurosci 24:3141–3152.

Wu S, Mehta SQ, Pichaud F, Bellen HJ, Quiocho FA (2005) Sec15 interacts with Rab11 via a novel domain and affects Rab11 localization in vivo. Nat Struct Mol Biol 12:879–885.

Xu F, Gainetdinov RR, Wetsel WC, Jones SR, Bohn LM, Miller GW, Wang YM, Caron MG (2000) Mice lacking the norepinephrine transporter are supersensitive to psychostimulants. Nat Neurosci 3:465–471.

Zadeh AD, Xu H, Loewen ME, Noble GP, Steele DF, Fedida D (2008) Internalized Kv1.5 traffics via Rab-dependent pathways. J Physiol 586:4793–4813.

Zerial M, McBride H (2001) Rab proteins as membrane organizers. Nat Rev Mol Cell Biol 2:107–117.

Zhang XM, Ellis S, Sriratana A, Mitchell CA, Rowe T (2004) Sec15 is an effector for the Rab11 GTPase in mammalian cells. J Biol Chem 279:43027–43034.